A Modular Adaptive Robust Nonlinear Control for Resilient Integration of VSIs Into Emerging Modernized Microgrids

Masoud Davari, *Senior Member, IEEE*, Mohammad Pourmahmood Aghababa, *Member, IEEE*, Frede Blaabjerg, *Fellow, IEEE*, and Mehrdad Saif, *Senior Member, IEEE*

***Abstract*— Nowadays, emerging modernized microgrids (MMGs) have significantly employed the voltage-source inverters (VSIs). VSIs are enabling technologies to form multi-infeed ac/dc (MIACDC) power systems integrating a variety of generation units and different loads into one coherent grid. In emerging MMGs, the frequency-dependent dynamics of multiple components affect the PQ-controlled, grid-connected VSIs (GC-VSIs), particularly when integrated into a weak network. In order to address this challenging problem, the full integration of the dynamics of the phase-locked loop (PLL) into those of GC-VSIs is accomplished in this research via an innovative modular structure to improve the VSI's performance. This action is expected to significantly reduce the effect of the ac-side dynamics on the control of GC-VSIs. In addition, there are uncertainties associated with the parameters in the system. Accordingly, mismatched disturbances and uncertainties (both matched and mismatched ones) will appear in a nonlinear dynamic problem, and therefore, from the standpoint of control theories, mismatched disturbances and uncertainties should be overcome. Satisfying them is a difficult task in control of nonlinear systems. Therefore, one of the main contributions of this work is finding an appropriate mathematical model of GC-VSIs in the dq-frame for the problem under study. Afterward, in order to control both active and reactive power independently, this article presents a novel two-degree-of-freedom (2DoF) methodology with an enhanced modular design. It combines the sliding-mode control with a "new sliding manifold" and a disturbance observer with a "new adaptation rule" taking care of uncertainties and mismatched disturbances. Those disturbance signals may be generated by the PLL dynamics or voltage signals affecting the GC-VSI's dynamics. Through providing mathematical analyses (including stability assessments via various theorems using Lyapunov stability criterion), simulation results, and experiments, this article demonstrates the effectiveness of the proposed control methodology. The industrially accepted GC-VSI equipped with an LCL-filter is used here.**

***Index Terms*— And uncertainties, disturbance observer, emerging grids, grid-connected voltage-source inverters (GC-VSIs), Lyapunov stability, mismatched disturbances, multi-infeed ac/dc (MIACDC) grids, phase-locked loop (PLL), sliding mode control (SMC).**

I. Introduction

THE energy sector has been significantly progressing and moving toward simultaneously integrating power networks and energy storage systems (e.g., battery systems) embedded in ac/dc grids. They are also called multi-infeed ac/dc (MIACDC) grids, which are used in both power transmission systems and electric power distribution [e.g., modernized microgrid (MMG) technology] under the umbrella of smart grids [1]–[5]. In smart grids, the modernized MIACDC concept brings many benefits to the operation, control, and demand supply within commercial power systems. MIACDC-based configurations will employ a new trend in its power architecture, suggested as a fully integrated power and energy system (FIPES) in this work, thanks to the integration of battery energy storage systems. FIPESs have a similar structure to what is employed in terrestrial power systems, but they highly integrate energy storage units—e.g., battery systems. FIPES needs consideration associated with the control methodologies of the MIACDC power systems. They employ a lot of voltage-source-converter-based systems, among which PQ-controlled, grid-connected voltage-source inverters (GC-VSIs) play a vital role in power flows and energy exchange in the MIACDC power structure.

PQ-controlled GC-VSIs exchange power between an ac grid and a stabilized dc link in FIPESs. From now on, PQ-controlled GC-VSIs are referred to as "GC-VSIs" herein. The weakness of the ac grid strongly affects the stability and performance of the GC-VSIs because of the grid impedance and the frequency dynamics, primarily provided that a dq-frame control method is applied (e.g., see [6] and references therein). The dynamics mentioned earlier will be coupled through the phase-locked loop (PLL) dynamics. Those

Manuscript received December 6, 2019; revised February 9, 2020; accepted March 10, 2020. Date of publication March 30, 2020; date of current version May 28, 2021. The work of Masoud Davari was supported by the U.S. National Science Foundation (NSF) via the Core Program of Energy, Power, Control, and Networks (EPCN) in the Division of Electrical, Communications and Cyber Systems (ECCS), under Grant 1902787 and Grant 1808279. Recommended for publication by Associate Editor Carl N. M. Ho. *(Corresponding author: Masoud Davari.)*

Masoud Davari is with the Department of Electrical and Computer Engineering, Allen E. Paulson College of Engineering and Computing, Georgia Southern University, Statesboro Campus, Statesboro, GA 30460 USA (e-mail: mdavari@georgiasouthern.edu; davari@ualberta.ca).

Mohammad Pourmahmood Aghababa is with the Department of Electrical Engineering, Urmia University of Technology, Urmia 5756151818, Iran, and also with the Department of Electrical and Computer Engineering, Faculty of Engineering, University of Windsor, Windsor, ON N9B 3P4, Canada (e-mail: m.p.aghababa@ee.uut.ac.ir; mp.aghababa@uwindsor.ca).

Frede Blaabjerg is with the Department of Energy Technology, Aalborg University, 9220 Aalborg, Denmark (e-mail: fbl@et.aau.dk).

Mehrdad Saif is with the Department of Electrical and Computer Engineering, Faculty of Engineering, University of Windsor, Windsor, ON N9B 3P4, Canada (e-mail: msaif@uwindsor.ca).

Color versions of one or more of the figures in this article are available online at https://ieeexplore.ieee.org.

Digital Object Identifier 10.1109/JESTPE.2020.2984231

dynamics affect the stability and performance of the overall MIACDC grid accordingly. Therefore, frequency-dependent detailed dynamics of various components and control aspects of the GC-VSIs in weak networks are required to be investigated thoroughly. They are mostly created either by the PLL equipped with various control strategies in weak grids because of the ac-side grid impedance [6]–[10].

Moreover, the control of GC-VSIs under different grid conditions has been studied and investigated in various research studies [5], [6], [11]–[24]. According to their research, because of the highly interconnected structure of FIPESs, there are a lot of mismatched disturbances and/or uncertainties, which are affecting the active/reactive power controls of GC-VSIs. Those disturbances and uncertainties impact the performance of active/reactive power controls—which finally influence the FIPES's power quality. It is especially essential when GC-VSIs are highly used as an alternative way of MMGs' integration into the primary grid soon (see [3] for further information on this promising approach). To the best of our knowledge, thus far, there has not been any solid research work on the effects of mismatched disturbances and/or uncertainties in control of the nonlinear dynamic system of GC-VSIs from the standpoint of a two-degree-of-freedom (2DoF) control. Besides, considering both "matched" and "mismatched" uncertainties of uncertain GC-VSI's dynamics for synthesizing a 2DoF modular control (to regulate both active and reactive power independently) is a must for fulfilling novel research on the GC-VSI controls. At the same time—because of benefiting from pulsewidth-modulation (PWM) schemes [11]—the input signals of the control system will be saturated, thus dealing with an input saturation problem in our control design.

While considering and dealing with both matched and mismatched uncertainties of uncertain 2DoF dynamic system of GC-VSIs with input saturation, the objective of this research is to develop a novel nonlinear adaptive modular control strategy and apply it to GC-VSIs. The intended nonlinear approach will be based on the sliding mode control (SMC) methodology because it is one of the most successful robust control techniques. As shown in [25], an SMC with a disturbance observer scheme can be used in overcoming mismatched disturbances and uncertainties in controlling mechanical systems. SMCs utilize a prescribed sliding surface and a switching control rule to persist against system uncertainties and external disturbances. This research will benefit from a novel SMC—which is able to handle mismatched uncertain terms although the original SMCs are not able to overcome system mismatched uncertainties [26]–[28]. Fundamentally, in order to take advantage of such a modular control system, a new sliding manifold merged with a new disturbance observer is required to be redesigned for GC-VSIs—which benefit from a modular structure. Consequently, designing an SMC with a new sliding manifold—including its rigorous stability—requires separate research conducted for the GC-VSIs. Furthermore, it is necessary to appropriately model and reformulate the GC-VSI's dynamics here.

The structure shown in [25] is regarded as one of the best candidates for the problem formulation in mechanical systems proposed there. Inspired by the control structure in [25], this article needs to introduce a new sliding manifold for redesigning an appropriate SMC for the electronic power problem under study. Therefore, it needs to provide proof of the rigorous stability of the new SMC. Then, a modified disturbance observer strategy is being used for enhancing the robustness of the system against matched and mismatched uncertainties, and a finite-time control technique is applied as an acceptable control strategy, which has appropriate disturbance rejection properties. At the same time, owing to the limited operation of the control inputs (equivalent to considering the saturation of a modulation index in PWM schemes), the practical implementations of GC-VSIs' control systems are faced with some typical input constraints. Studies in power electronics (see [11], [12], [29], [30]) have shown that PWM schemes can cause different nonlinearities because of overmodulation and saturations. This constraint is well known that saturation is one of the commonly occurred nonlinearities in control systems. Therefore, the PWM's modulation indices can lead to severe control deterioration or even make an instability state for the system. This observation gets worse and drastically appears when dealing with weak grids—where a PLL captures the frequency dynamics [7]. In other words, neglecting the effects of the PWM's modulation indices either can lead to deterioration of the control performance, can produce some oscillations in the system output with delays, or even result in a system failure. These possible adverse impacts are because of not considering the saturation of the control input in the control design stage as one of the nonlinear terms and limitations of control input.

Considering the problems detailed earlier, the key contributions of this article are listed as follows.

1) It proposes a 2DoF control design approach for GC-VSIs—based on the PQ-controlled GC-VSIs' need to control active and reactive power as 2DoF—similar to what exists in robotic and mechanical systems.
2) It synthesizes a novel "modular" nonlinear SMC strategy for GC-VSIs, which is able to effectively deal with a critical control problem associated with both matched and mismatched model uncertainties and low and fast external disturbances.
3) It accomplishes a powerful combination of the PLL dynamics with the GC-VSI control to address the challenging problem of the integration of GC-VSIs into weak grids. Then, the proposed modular architecture significantly reduces the impacts of the ac-side dynamics on the active/reactive power control of GC-VSIs.
4) It identifies the system uncertainties and external disturbances. Here, it is supposed that the bounds of the uncertain terms and external disturbance are unknown; this assumption is rational enough, practically. It additionally compensates for the effects of the perturbations via a disturbance observer using a new adaptation rule—which is proposed in this research. Therefore, the synthesized adaptive observer guarantees robustness against changes in the disturbances signals and prevents having restrictions on the disturbances, e.g., type, amplitude, and so on.

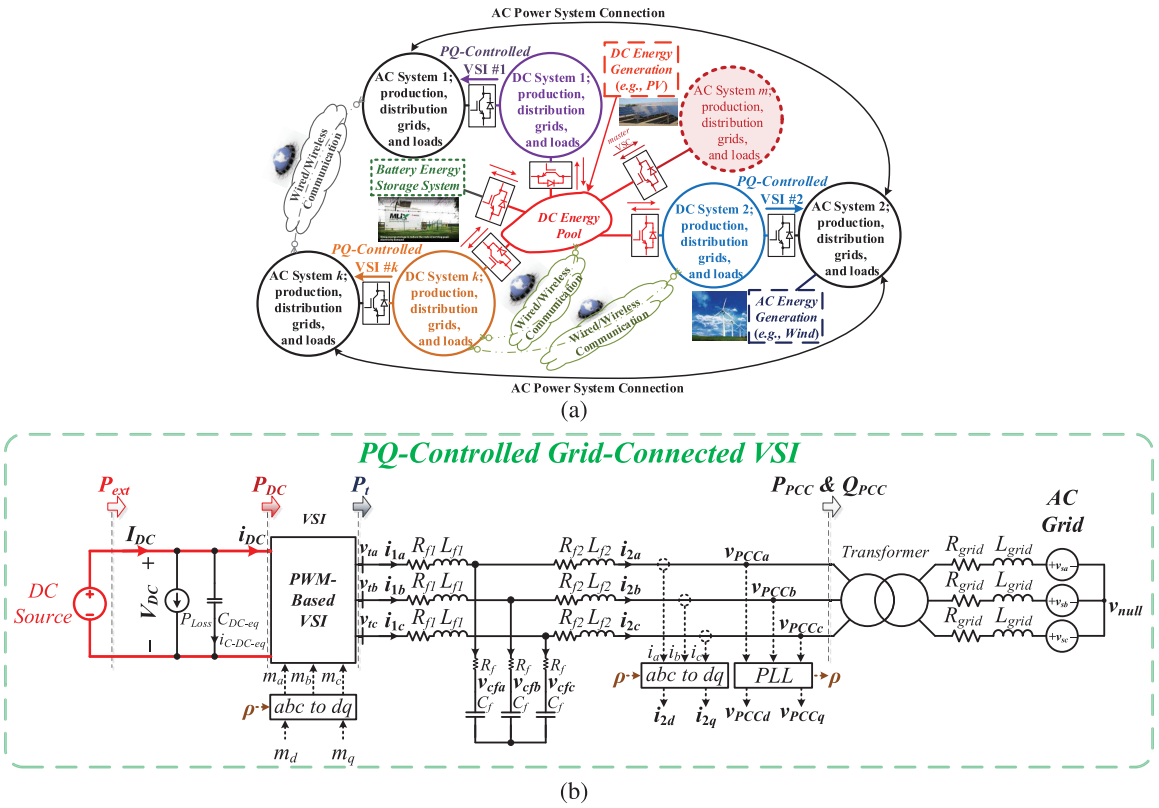

Fig. 1. (a) Notional structure of an MIACDC power architecture. (b) Block diagram of the proposed control scheme for GC-VSIs.

5) Last but not least, it looks at the nonlinearities made by the PWM scheme and includes a mechanism to consider them in the control structure through an analytical approach. In this regard, the input control is assumed to be disturbed by unknown saturation nonlinearity. Indeed, this approach also takes into account the nonlinearities made by the PWM scheme. This way, their influences are also seen in the control structure, thus improving the performance mathematically.

The remaining parts of this article are organized as follows. In Section II, this study formulates an appropriate model for GC-VSI's dynamics with both matched and mismatched uncertainties and mismatched disturbances. Section III proposes a 2DoF control for GC-VSIs with an enhanced modular design combining SMC (with the proposed sliding manifold) and disturbance observer considering the saturation of a modulation index, along with a control technique based on the "finite-time stable equilibrium point." In order to reveal the effectiveness of the proposed control algorithm, in Sections IV and V, simulations and experiments have been provided. Finally, Section VI gives the conclusions.

II. Mathematical Model of GC-VSIs for Designing an SMC With 2DoF

A notional architecture of an MIACDC's power grid (both power and communication one) has been shown in Fig. 1(a). As shown in Fig. 1(a), many power electronic links should work as GC-VSIs transferring power from dc side to the ac side, e.g., VSI #1, VSI #2, and VSI #k in Fig. 1(a). Fig. 1(b) shows the structure of a GC-VSI with an LCL-filter, which is very industrially accepted [17], [31]. Using Kirchhoff's circuit laws for the average model in Fig. 1(b), the results in the average dynamics of the system using space-phasor representation are described by (1) [12], [27]

$$\begin{cases} \vec{v}_t - (\vec{v}_{cf} + R_f(\vec{i}_1 - \vec{i}_2)) = L_{f1}\dfrac{d\vec{i}_1}{dt} + R_{f1}\vec{i}_1 \\ (\vec{v}_{cf} + R_f(\vec{i}_1 - \vec{i}_2)) - \vec{v}_{\rm PCC} = L_{f2}\dfrac{d\vec{i}_2}{dt} + R_{f2}\vec{i}_2 \\ \vec{i}_1 - \vec{i}_2 = C_f\dfrac{d\vec{v}_{cf}}{dt} \end{cases} \tag{1}$$

where $\vec{i}_1$ is the space phasor representing the converter-side currents of i_{1a}, i_{1b}, and i_{1c}, $\vec{i}_2$ is the space phasor representing the ac-grid-side, i.e., the point of common coupling (PCC), currents of i_{2a}, i_{2b}, and i_{2c}, $\vec{v}_{\rm cf}$ is the space phasor representing the capacitor voltages of $v_{\rm cfa}$, $v_{\rm cfb}$, and $v_{\rm cfc}$, $\vec{v}_{\rm PCC}$ is the space phasor representing the PCC voltages of $v_{\rm PCCa}$, $v_{\rm PCCb}$, and $v_{\rm PCCc}$, L_{f1}/R_{f1} is the LCL-filter's converter-side inductance/resistance, L_{f2}/R_{f2} is LCL-filter's ac-grid-side inductance/resistance, and C_f is the LCL-filter's shunt capacitance—all shown in Fig. 1, where C_f's resistance of R_f is negligible compared with C_f's impedance (i.e., 50× and larger).

After finding $\vec{i}_1$ with respect to $\vec{i}_2$ from the third part of (1) and substituting $\vec{i}_1$ with that and also after finding $\vec{v}_{\rm cf}$ with respect to $\vec{v}_{\rm PCC}$ from the second part of (1) and substituting

$\vec{v}_{\rm cf}$ with that, the first part of (1) is obtained as follows:

$$\begin{aligned}\vec{v}_t = &\underbrace{(L_{f1}R_{f2}C_f + L_{f2}R_{f1}C_f + L_{f1}R_fC_f)}_{\triangleq A}\frac{d^2\vec{i}_2}{dt^2}\\ &+\underbrace{(L_{f1}+L_{f2}+R_{f1}R_{f2}C_f + R_{f1}R_fC_f)}_{\triangleq B}\frac{d\vec{i}_2}{dt}\\ &+\underbrace{(R_{f1}+R_{f2})}_{\triangleq \Gamma}\vec{i}_2 + \underbrace{(L_{f1}C_f + R_f^2C_f^2)}_{\triangleq E}\frac{d^2\vec{v}_{\rm PCC}}{dt^2}\\ &+\underbrace{(R_{f1}C_f + R_fC_f)}_{\triangleq H}\frac{d\vec{v}_{\rm PCC}}{dt} + \vec{v}_{\rm PCC}. \end{aligned} \tag{2}$$

After mathematical manipulations, which, for example, can be found in [6] and [12], (3) is found by expressing (2) in the well-known rotating dq-frame

$$\begin{cases}\dfrac{d^2i_{2d}}{dt^2} = 2\omega\dfrac{di_{2q}}{dt} + \omega^2 i_{2d} + \dfrac{d\omega}{dt}i_{2q} - \dfrac{B}{A}\dfrac{di_{2d}}{dt} + \dfrac{B}{A}\omega i_{2q}\\ \qquad -\dfrac{\Gamma}{A}i_{2d} - \dfrac{E}{A}\dfrac{d^2v_{\rm PCCd}}{dt^2} + \dfrac{E}{A}2\omega\dfrac{dv_{\rm PCCq}}{dt}\\ \qquad +\dfrac{E}{A}\omega^2 v_{\rm PCCd} + \dfrac{E}{A}\dfrac{d\omega}{dt}v_{\rm PCCq} - \dfrac{H}{A}\dfrac{dv_{\rm PCCd}}{dt}\\ \qquad +\dfrac{H}{A}\omega v_{\rm PCCq} - \dfrac{1}{A}v_{\rm PCCd} + \dfrac{1}{A}v_{t_d},\\ \dfrac{d^2i_{2q}}{dt^2} = -2\omega\dfrac{di_{2d}}{dt} + \omega^2 i_{2q} - \dfrac{d\omega}{dt}i_{2d} - \dfrac{B}{A}\dfrac{di_{2q}}{dt} - \dfrac{B}{A}\omega i_{2d}\\ \qquad -\dfrac{\Gamma}{A}i_{2q} - \dfrac{E}{A}\dfrac{d^2v_{\rm PCCq}}{dt^2} - \dfrac{E}{A}2\omega\dfrac{dv_{\rm PCCd}}{dt}\\ \qquad +\dfrac{E}{A}\omega^2 v_{\rm PCCq} - \dfrac{E}{A}\dfrac{d\omega}{dt}v_{\rm PCCd} - \dfrac{H}{A}\dfrac{dv_{\rm PCCq}}{dt}\\ \qquad -\dfrac{H}{A}\omega v_{\rm PCCd} - \dfrac{1}{A}v_{\rm PCCq} + \dfrac{1}{A}v_{t_q}\end{cases} \tag{3}$$

where i_{2d}/i_{2q} is the d-/q- component of $\vec{i}_2$, and $v_{\rm PCCd}/v_{\rm PCCq}$ are d-/q- component of $\vec{v}_{\rm PCC}$, respectively.

For the control design, (3) is able to describe the GC-VSI's dynamics. In this regard, in order to include the GC-VSI's mismatched uncertainties and external disturbances suited to the 2DoF control design process, the following state-space equation is acquired. Equation (4), as shown at the bottom of the next page, is able to mathematically describe the aforementioned mismatched uncertainties and external disturbances as required for the control design in this article, where x_1 defines i_{2d}; x_2 defines $\dot{i}_{2d}$; x_3 defines i_{2q}; x_4 defines $\dot{i}_{2q}$; ω is the angular frequency provided by the PLL; $\mathcal{N}_k(.)$—which is the saturation function associated with the PWM strategy—and the rest of variable have been defined in (2).

Considering (4), (5) is obtained. It is noteworthy that (5) is based on the general model required for employing the general structure in [25]. Equation (5) is able to include the GC-VSI's mismatched uncertainties and external disturbances suited to the 2DoF control design process, which will be discussed more in Section III-A

$$\begin{cases}\dot{x}_1 = x_2 + \Delta f_1(X,t)\\ \dot{x}_2 = f_1(X,t) + \Delta f_2(X,t) + d_2(t) + \mathcal{N}_1(u_1(t))\\ \dot{x}_3 = x_4 + \Delta f_3(X,t)\\ \dot{x}_4 = f_2(X,t) + \Delta f_4(X,t) + d_4(t) + \mathcal{N}_2(u_2(t))\end{cases} \tag{5}$$

where $\Delta f_1(X,t)$ is the mismatched uncertainty affecting x_1, $\Delta f_2(X,t)$ is the matched uncertainty affecting x_2, $d_2(t)$ is the external disturbance impacting on x_2's dynamics, $\Delta f_3(X,t)$ is the mismatched uncertainty affecting x_3, $\Delta f_4(X,t)$ is the matched uncertainty affecting x_4, and $d_4(t)$ is the external disturbance impacting x_4's dynamics.

III. Proposed Methodology

Based on Section II and the mathematical model provided by (4) and (5), this article needs to introduce a novel nonlinear SMC modular strategy merged with a disturbance observer for GC-VSIs. The proposed approach helps GC-VSIs be able to deal with both matched and mismatched model uncertainties and low and fast external disturbances, for resilient operation. Fig. 2 shows a notional structure of the controller, which is required in this type of problem formations, based on [25]. However, the sliding manifold should be "re"designed, and a new adaptation rule is required to reintroduced in this work.

In order to compensate the perturbations' effects—whose majorities are PLL dynamics and grid voltage—a disturbance observer (integrated into the SMC) is employed to recognize the system uncertainties and external disturbances. For complying with practical scenarios, it is presumed that the uncertain terms' bounds and the bound of external disturbance are unknown beforehand. A twofold sliding manifold with desired properties—i.e., a quick convergence behavior and no steady-state error—is then required to be designed for the GC-VSI accordingly.

A. Mathematical Formulation

Based on our need for designing a 2DoF modular controller associated with (4) and (5), a generalized dynamic system is considered as follows:

$$\begin{cases}\dot{x}_{2k-1}(t) = x_{2k}(t) + \Delta f_{2k-1}(X,t) + d_{2k-1}(t)\\ \dot{x}_{2k}(t) = f_k(X,t) + \Delta f_{2k}(X,t) + d_{2k}(t) + (b_k(X,t)\\ \qquad\qquad + \Delta b_k(X,t))\mathcal{N}_k(u_k(t))\end{cases} \tag{6}$$

where $k = 1, 2$, $X(t) = [x_1(t), x_2(t), x_3(t), x_4(t)]^T \in \mathbb{R}^4$ is the state vector of the system, $\Delta f_{2k-1}(X,t) \in \mathbb{R}^{4\times 1} \times \mathbb{R}^+ \to \mathbb{R}$ and $d_{2k-1}(t) \in \mathbb{R}^+ \to \mathbb{R}$ are mismatched uncertainties and external disturbances, respectively, $f_k(X,t) \in \mathbb{R}^{4\times 1} \times \mathbb{R}^+ \to \mathbb{R}$ is a continuous function modeling the nonlinear dynamics of the $k^{\rm th}$ part of the system, $\Delta f_{2k}(X,t) \in \mathbb{R}^{4\times 1} \times \mathbb{R}^+ \to \mathbb{R}$ and $d_{2k}(t) \in \mathbb{R}^+ \to \mathbb{R}$ are matched uncertainties and external disturbances, respectively, $b_k(X,t) \in \mathbb{R}^{4\times 1} \times \mathbb{R}^+ \to \mathbb{R}$ is the time-varying gain of the control input (if any), $\Delta b_k(X,t) \in \mathbb{R}^{4\times 1} \times \mathbb{R}^+ \to \mathbb{R}$ denotes the variations of the control signal (if any), $\mathcal{N}_k(.)$ can either be a linear function or be a nonlinear saturation function, and $u_k(t) \in \mathbb{R}$ is the control input.

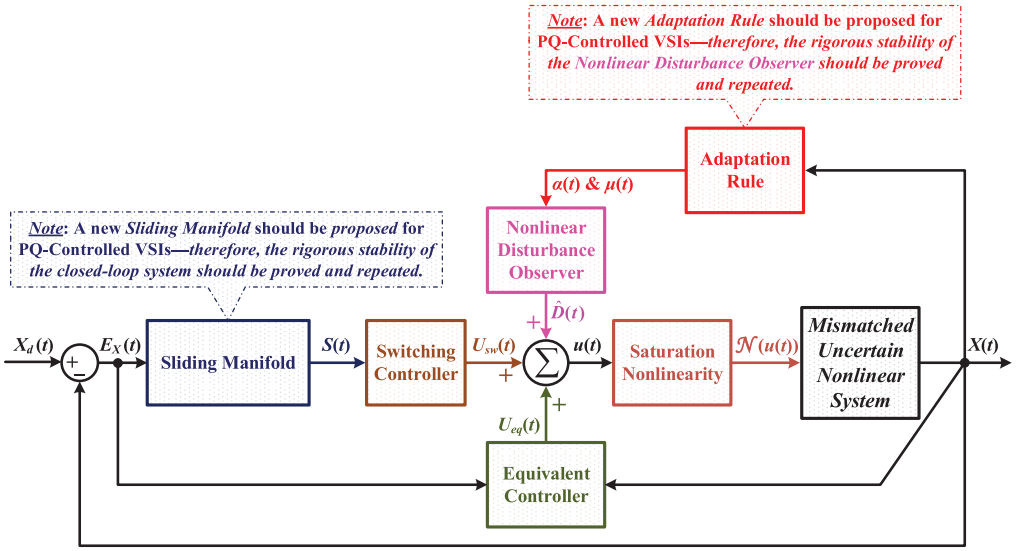

Fig. 2. Block diagram of the modular control scheme for GC-VSIs in the state-space representation.

It is supposed that a smooth desired state trajectory in the form of $X(t) = [x_{d1}(t), x_{d2}(t), x_{d3}(t), x_{d4}(t)]^T$ exists. Therefore, by defining the tracking error as $E(t) = X(t) - X_d(t) = -E_x(t)$, (7) is able to obtain the tracking error dynamics as described in the following:

$$\begin{cases} \dot{e}_{2k-1}(t) = e_{2k}(t) + x_{d2k}(t) - \dot{x}_{d2k-1}(t) + \Delta f_{2k-1}(X,t) \\ \qquad\qquad + d_{2k-1}(t) \\ \dot{e}_{2k}(t) = f_k(X,t) - \dot{x}_{d2k}(t) + \Delta f_{2k}(X,t) \\ \qquad\qquad + d_{2k}(t) + [b_k(X,t) + \Delta b_k(X,t)]\mathcal{N}_k(u_k(t)) \end{cases} \tag{7}$$

where $k = 1, 2$.

In order to design an adaptive disturbance observer, a new function is needed to be defined as follows. Regarding $D_k(X,u,t) = \Delta f_{2k-1}(X,t) + d_{2k-1}(t) + \Delta \dot{f}_{2k-1}(X,t) + \dot{d}_{2k-1}(t) + \Delta f_{2k}(X,t) + d_{2k}(t) + \Delta b_k(X,t)\mathcal{N}_k(u_k(t))$ as the lumped perturbation, it is assumed that constants $\alpha_k, \mu_k \in \mathbb{R}^+$ exists such that

$$\|D_k(X,u,t)\| \le \alpha_k |\delta_k| + \mu_k \tag{8}$$

where $k = 1, 2$; $\Delta \dot{f}_{2k-1}(X,t)$ is defined as $\sum_{j=1}^{4}((\partial \Delta f_{2k-1}(X,t))/\partial x_j)\dot{x}_j + ((\partial \Delta f_{2k-1}(X,t))/\partial t)$; α_k and μ_k are unknown values, and δ_k is a function of state errors (will be defined in Section III-C).

$$\begin{cases} \dot{x}_1 = x_2 + \Delta f_1(X,t), \\ \dot{x}_2 = \underbrace{\left(\omega^2 - \dfrac{\Gamma}{A}\right)x_1 + \dfrac{-B}{A}x_2 + \left(\dfrac{B}{A}\omega + \dfrac{d\omega}{dt}\right)x_3 + 2\omega x_4 + \Delta f_2(X,t)}_{\triangleq f_1(X,t)}, \\ \qquad + \underbrace{\dfrac{-E}{A}\dfrac{d^2 v_{\mathrm{PCC}d}}{dt^2} + \dfrac{2E}{A}\omega\dfrac{dv_{\mathrm{PCC}q}}{dt} + \dfrac{E}{A}\omega^2 v_{\mathrm{PCC}d} + \dfrac{E}{A}\dfrac{d\omega}{dt}v_{\mathrm{PCC}q} + \dfrac{-H}{A}\dfrac{dv_{\mathrm{PCC}d}}{dt} + \dfrac{H}{A}\omega v_{\mathrm{PCC}q} + \dfrac{-1}{A}v_{\mathrm{PCC}d}}_{\triangleq d_2(t)} \\ \qquad + \underbrace{\dfrac{0.5V_{dc}}{A}}_{\triangleq b_1}\mathcal{N}(\underbrace{m_d}_{\triangleq u_1}), \\ \dot{x}_3 = x_4 + \Delta f_3(X,t), \\ \dot{x}_4 = \underbrace{\left(\dfrac{-B}{A}\omega - \dfrac{d\omega}{dt}\right)x_1 + (-2\omega)x_2 + \left(\omega^2 - \dfrac{\Gamma}{A}\right)x_3 + \dfrac{-B}{A}x_4 + \Delta f_4(X,t)}_{\triangleq f_2(X,t)}, \\ \qquad + \underbrace{\dfrac{-E}{A}\dfrac{d^2 v_{\mathrm{PCC}q}}{dt^2} + \dfrac{-2E}{A}\omega\dfrac{dv_{\mathrm{PCC}d}}{dt} + \dfrac{E}{A}\omega^2 v_{\mathrm{PCC}q} + \dfrac{-E}{A}\dfrac{d\omega}{dt}v_{\mathrm{PCC}d} + \dfrac{-H}{A}\dfrac{dv_{\mathrm{PCC}q}}{dt} + \dfrac{-H}{A}\omega v_{\mathrm{PCC}d} + \dfrac{-1}{A}v_{\mathrm{PCC}q}}_{\triangleq d_4(t)} \\ \qquad + \underbrace{\dfrac{0.5V_{dc}}{A}}_{\triangleq b_2}\mathcal{N}(\underbrace{m_q}_{\triangleq u_2}) \end{cases} \tag{4}$$

Remark 1: It is noteworthy that terms associated with both of the matched and mismatched uncertainties and external disturbances are always bounded in GC-VSIs. Also, having a finite magnitude is necessary for the designed control input. Therefore, it is concluded that the assumption and the conditions mentioned earlier are realistic for this research, thus not restricting our practical scenarios.

Remark 2: As demonstrated in Fig. 2, this article's control goal is to propose and synthesize a "new sliding manifold" for the selected control structure. It also employed the SMC combined with a disturbance observer (using an adaptation rule) for the 2DoF system of GC-VSIs with matched and mismatched uncertainties [i.e., (4) and (5)], in addition to saturated control inputs. Besides, for the disturbance observer, the unknown terms' bounds have to be determined by a "new adaption law," which should be proposed. As both of the manifold and adaptation rules change here, a new proof is required for the rigorous stability of the closed-loop system, which is augmented with the disturbance observer described in the following.

B. SMC With the Proposed Sliding Manifold

A twofold terminal sliding manifold is required to be "re"synthesized so that the structure can be adopted for the problem formulation here. As regards this, a first-fold and a second-fold of the sliding manifold have been proposed as follows:

$$\begin{cases} s_{2k-1}(t) = e_{2k-1}(t) \\ \qquad + \int_0^t (e_{2k-1}(\tau) + \eta_k \text{sign}(e_{2k-1}(\tau)))d\tau \\ s_{2k}(t) = \dot{s}_{2k-1}(t) \\ \qquad + \int_0^t (\gamma_{k\text{-}a}\text{sign}(s_{2k-1}(\tau))|s_{2k-1}(\tau)|^{a_{k\text{-}a}} \\ \qquad\quad + \gamma_{k\text{-}b}\text{sign}(\dot{s}_{2k-1}(\tau))|\dot{s}_{2k-1}(\tau)|^{a_{k\text{-}b}})d\tau \end{cases} \tag{9}$$

where $\eta_k > 0$, $\gamma_{k\text{-}a} > 0$, $\gamma_{k\text{-}b} > 0$, $0 < a_{k\text{-}a} < 1$, and $0 < a_{k\text{-}b} < 1$ are constant values, and $k = 1, 2$.

The condition of $s = 0$ is met once the system operates in the sliding mode, which is based on the SMC theory. Taking into account this property—from (9) as the new sliding manifold proposed—the following sliding-mode dynamics is obtained. In *Theorem* 1, it has been proven that, considering (9) as the proposed sliding manifold, "zero" is the finite-time stable equilibrium point of the nonsmooth sliding-mode dynamics (10)

$$\begin{cases} s_{2k-1} = 0 \Rightarrow \dot{s}_{2k-1} = 0 \\ \quad \Longrightarrow \dot{e}_{2k-1} = -(e_{2k-1} + \eta_k \text{sign}(e_{2k-1})) \\ s_{2k} = 0 \Rightarrow \dot{s}_{2k} = 0 \\ \quad \Longrightarrow \ddot{s}_{2k-1} = -(\gamma_{k\text{-}a}\text{sign}(s_{2k-1})|s_{2k-1}|^{a_{k\text{-}a}} \\ \qquad\qquad + \gamma_{k\text{-}b}\text{sign}(\dot{s}_{2k-1})|\dot{s}_{2k-1}|^{a_{k\text{-}b}}) \end{cases} \tag{10}$$

where $k = 1, 2$.

Theorem 1 (Finite-Time Stable Equilibrium Point of the Proposed Sliding Mode Dynamics): The stable equilibrium point of the nonsmooth sliding-mode dynamics (10) is "zero" (in the finite-time manner).

Proof: For $s_{2k-1} = 0$: By defining $V^a_{2k-1}(t) = 0.5e^2_{2k-1}(t)$ as a candidate for the Lyapunov function, the following expression for $\dot{V}^a_{2k-1}(t)$ is achieved:

$$\dot{V}^a_{2k-1}(t) = e_{2k-1}(t)\dot{e}_{2k-1}(t). \tag{11}$$

As a result of inserting $\dot{e}_{2k-1}(t)$ from (10) into (11), $\dot{V}^a_{2k-1}(t)$ is formulated as

$$\begin{aligned} \dot{V}^a_{2k-1}(t) &= -e_{2k-1}(t)(e_{2k-1} + \eta_k \text{sign}(e_{2k-1})) \\ &= -\left(e^2_{2k-1}(t) + \eta_k|e_{2k-1}|\right) \le -\eta_k|e_{2k-1}| \\ &\Rightarrow \dot{V}^a_{2k-1}(t) \le 0. \end{aligned} \tag{12}$$

Consequently, the earlier shows that the sliding-mode dynamics are globally asymptotically stable. By taking integral from (12)—on both sides—from the "reaching time" of $t_{2k-1,r}$ to the "stopping time" of $t_{2k-1,s}$, the following expression is gained [note that $V^a_{2k-1}(t_{2k-1,s}) = 0$]:

$$\begin{aligned} &\dot{e}_{2k-1}(t_{2k-1,r})\text{sign}(e_{2k-1}(t_{2k-1,r})) \le -\eta_k \\ &\qquad \Rightarrow t_{2k-1,s} \le \frac{|e_{2k-1}(t_{2k-1,r})|}{\eta_k} + t_{2k-1,r}. \end{aligned} \tag{13}$$

As a result of (13), the convergence to zero is absolute and will occur within a finite time.

For $s_{2k} = 0$: Here, auxiliary variables of $s_{2k-1} \triangleq s^a_{2k-1}$ and $\dot{s}_{2k-1} \triangleq s^b_{2k-1}$ are employed to describe the dynamics of $\ddot{s}_{2k-1}$ expressed in (10) as

$$\begin{cases} \dot{s}^a_{2k-1} = s^b_{2k-1}, \\ \dot{s}^b_{2k-1} = -\left(\gamma_{k\text{-}a}\text{sign}\left(s^a_{2k-1}\right)\left|s^a_{2k-1}\right|^{a_{k\text{-}a}}\right. \\ \qquad\qquad \left. + \gamma_{k\text{-}b}\text{sign}\left(s^b_{2k-1}\right)\left|s^b_{2k-1}\right|^{a_{k\text{-}b}}\right). \end{cases} \tag{14}$$

Therefore, according to [32], the point of $s^a_{2k-1} = s^b_{2k-1} = 0$ is the finite-time stable equilibrium point provided that parameters of the sliding manifold are selected to satisfy the following conditions, which are $\gamma_{k\text{-}a} > 0$, $\gamma_{k\text{-}b} > 0$, $a_{k\text{-}a} = (a_{k\text{-}b}/(2 - a_{k\text{-}b}))$, $a_{k\text{-}b} \in (1 - \epsilon, 1)$, and $\epsilon \in (0, 1)$. Both of the parts mentioned earlier lead to ending the proof. □

C. Disturbance Observer With the Proposed Adaption Rule

In this section, the proposed modular control design combining SMC methodology modulated combined with a disturbance observer is introduced. Here, the structure of [25] is redesigned so that it is applicable to GC-VSIs considering a new form of (8). In order to originate a disturbance observer—which is suitable for the nonlinear error system (7)—the auxiliary variable of $\delta_k(t)$ is considered as expressed in the following:

$$\delta_k(t) = e_{2k-1}(t) + \dot{e}_{2k-1}(t) - z_k(t), \quad \text{for } k = 1, 2 \tag{15}$$

where $z_k(t)$ is calculated by the following dynamic equation:

$$\begin{cases} \dot{z}_k(t) = b_k(X, t)\mathcal{N}_k(u_k(t)) - \psi_k \\ \psi_k = -[(\beta_k + \hat{\alpha}_k)\delta_k + \hat{\mu}_k \text{sign}(\delta_k) + f_k(X, t) + e_{2k}(t) \\ \qquad + x_{d2k}(t) - \dot{x}_{d2k-1}(t) - \ddot{x}_{d2k-1}(t)] \\ \dot{\hat{\alpha}}_k = h_k\delta^2_k \end{cases} \tag{16}$$

where $\beta_k > 0$ and $h_k > 0$ are constant values for the design process, and $\hat{\alpha}_k$ is an adaptive parameter for variable α_k. Besides, $\hat{\mu}_k$ is updated via the following adaption rule of:

$$\dot{\hat{\mu}}_k = p_k|\delta_k| \tag{17}$$

in which $p_k > 0$ is a constant gain.

Through expressing $\hat{D}_k(X,u,t)$ by $\hat{D}_k(X,u,t) = -(e_{2k}(t) + x_{d2k}(t) - \dot{x}_{d2k-1}(t) + f_k(X,t) - \ddot{x}_{d2k-1}(t) + \psi_k)$, the dynamics of δ_k is found as follows while assuming that the time derivatives of $D_k(X,u,t)$ and $\hat{D}_k(X,u,t)$ are bounded without loss of generality:

$$\dot{\delta}_k(t) = D_k(X,u,t) - \hat{D}_k(X,u,t), \quad \text{for } k = 1,2. \tag{18}$$

Theorem 2 (Observer Stability): The observer (18) has the global stable equilibrium point at "Zero"—although $D_k(X,u,t)$ gets into an unknown bound.

Remark 3: As there are new limit for the disturbance [i.e., (8)] and adaptation rule of (17), the proof of *Theorem 1* in [25] is not valid anymore. Therefore, a new proof is provided in the following.

Proof: The following function is selected as a candidate for the Lyapunov function:

$$V_k^b(t) = 0.5\delta_k^2(t) + \frac{0.5}{h_k}(\alpha_k - \hat{\alpha}_k)^2 + \frac{0.5}{p_k}(\mu_k - \hat{\mu}_k)^2. \tag{19}$$

Then, the derivative of the $V_k^b(t)$ mentioned above, with respect to time, is taken as described by

$$\dot{V}_k^b(t) = \dot{\delta}_k(t)\delta_k(t) - \frac{\dot{\hat{\alpha}}_k}{h_k}(\alpha_k - \hat{\alpha}_k) - \frac{\dot{\hat{\mu}}_k}{p_k}(\mu_k - \hat{\mu}_k). \tag{20}$$

After mathematical manipulations using $\dot{\hat{\alpha}}$ in (16), $\dot{\hat{\mu}}$ in (17), and $\dot{\delta}(t)$ in (18) and inserting them into (20), $\dot{V}_k^b(t)$ is described by

$$\begin{aligned}\dot{V}_k^b(t) = \delta_k(t)[&e_{2k}(t) + x_{d2k}(t) - \dot{x}_{d2k-1}(t) + f_k(X,t) \\ &- \ddot{x}_{d2k-1} + \psi_k + D_k(x,u,t)] - \delta_k^2(t)(\alpha_k - \hat{\alpha}_k) \\ &- |\delta_k(t)|(\mu_k - \hat{\mu}_k).\end{aligned} \tag{21}$$

From (21), it is now clear that

$$\begin{aligned}\dot{V}_k^b(t) \le \delta_k(t)[&e_{2k}(t) + x_{d2k}(t) - \dot{x}_{d2k-1}(t) + f_k(X,t) \\ &- \ddot{x}_{d2k-1} + \psi_k] + |\delta_k(t)|\|D_k(x,u,t)\| \\ &- \delta_k^2(t)(\alpha_k - \hat{\alpha}_k) - |\delta_k(t)|(\mu_k - \hat{\mu}_k).\end{aligned} \tag{22}$$

Afterward, using the assumptions made about $D_k(x,u,t)$ in (8), (22) is expressed and (23) is expressed as

$$\begin{aligned}\dot{V}_k^b(t) \le \delta_k(t)[&e_{2k}(t) + x_{d2k}(t) - \dot{x}_{d2k-1}(t) + f_k(X,t) \\ &- \ddot{x}_{d2k-1} + \psi_k] + \delta_k^2(t)\alpha_k + |\delta_k(t)|\mu_k \\ &- \delta_k^2(t)(\alpha_k - \hat{\alpha}_k) - |\delta_k(t)|(\mu_k - \hat{\mu}_k).\end{aligned} \tag{23}$$

Next, by substituting ψ_k from (16) into (23), the inequality (23) is found as

$$\begin{aligned}&\dot{V}_k^b(t) \\ &\le \delta_k(t)[e_{2k}(t) + x_{d2k}(t) - \dot{x}_{d2k-1}(t) + f_k(X,t) \\ &\quad - \ddot{x}_{d2k-1} - [(\beta_k + \hat{\alpha}_k)\delta_k + \hat{\mu}_k\text{sign}(\delta_k) + f_k(X,t) \\ &\qquad + e_{2k}(t) + x_{d2k}(t) - \dot{x}_{d2k-1}(t) - \ddot{x}_{d2k-1}(t)]] \\ &\quad + \delta_k^2(t)\hat{\alpha}_k + |\delta_k(t)|\hat{\mu}_k.\end{aligned} \tag{24}$$

Now, considering this fact that $\delta_k\text{sign}(\delta_k) = |\delta_k|$, $\dot{V}_k^b(t)$ is described by

$$\begin{aligned}\dot{V}_k^b(t) \le\ &-\delta_k(t)[(\beta_k + \hat{\alpha}_k)\delta_k(t) + \delta_k^2(t)\hat{\alpha}_k - |\delta_k(t)|\hat{\mu}_k \\ &+ \hat{\mu}_k|\delta_k(t)|] \\ \Rightarrow\ &\dot{V}_k^b(t) \le -\beta_k\delta_k^2(t) \le 0.\end{aligned} \tag{25}$$

Equation (25) proves that the origin is an asymptotic equilibrium point of the system (18), and therefore, it means that $\lim_{t\to\infty}\delta_k(t) = 0$.

Finally, based on Barbalat's lemma (see [33]), the assumptions made about the time derivatives of $D_k(X,u,t)$ and $\hat{D}_k(X,u,t)$ (which say that they are bounded without loss of generality). It is then concluded that $\lim_{t\to\infty}\dot{\delta}_k(t) = 0 \Rightarrow \lim_{t\to\infty}[D_k(X,u,t) - \hat{D}_k(X,u,t)] = 0$, which ensures that the observer error $[D_k(X,u,t) - \hat{D}_k(X,u,t)]$ asymptotically gains "zero" and concludes the proof. □

D. Control Design Considering Input Saturation

PWM is used in this research, and therefore, it imposes saturation limit on the control input. As a consequence, a revised SMC rule is required with the function $\mathcal{N}_k(.)$, which is a general nonlinear saturation function defined through [25], that is,

$$\mathcal{N}_k(u_k(t)) = \begin{cases} u_k^U, & \text{if } u_k(t) \ge u_k^u \\ \theta_k u_k(t), & \text{if } u_k^l \le u_k(t) \le u_k^u \\ u_k^L, & \text{if } u_k(t) \le u_k^l \end{cases} \tag{26}$$

where $k = 1,2$, u_k^U & $u_k^u \in \mathbb{R}^+$ and u_k^L & $u_k^l \in \mathbb{R}^-$ are the saturation function's bounds, and $\theta_k \in \mathbb{R}$ is the slope of saturation functions. Since it is supposed that all the saturation function's parameters [in (26)] are bounded and unknown in advance, the saturation function (26) can be rewritten in the form of (27)

$$\mathcal{N}_k(u_k(t)) = u_k(t) + \Delta u_k(u_k(t)) \tag{27}$$

where $k = 1,2$, and $\Delta u_k(u_k(t))$ is given by

$$\Delta u_k(u_k(t)) = \begin{cases} u_k^U - u_k(t), & \text{if } u_k(t) \ge u_k^u \\ (\theta_k - 1)u_k(t), & \text{if } u_k^l \le u_k(t) \le u_k^u \\ u_k^L - u_k(t), & \text{if } u_k(t) \le u_k^l. \end{cases} \tag{28}$$

Based on (27), the tracking error dynamics expressed in (7) can be rewritten as

$$\begin{cases} \dot{e}_{2k-1}(t) = e_{2k}(t) + x_{d2k}(t) - \dot{x}_{d2k-1}(t) + \Delta f_{2k-1}(X,t) \\ \qquad\qquad + d_{2k-1}(t) \\ \dot{e}_{2k}(t) = f_k(X,t) - \dot{x}_{d2k}(t) + \Delta f_{2k}(X,t) + d_{2k}(t) \\ \qquad\qquad + [b_k(X,t) + \Delta b_k(X,t)][u_k(t) + \Delta u_k(u_k(t))] \end{cases} \tag{29}$$

where $k = 1,2$.

Using the assumption that the upper bound of the lumped perturbation (i.e., α_k and μ_k) is unknown and the boundedness requirement for the practical control signals, it is concluded that the uncertain term $\Delta u_k(u_k(t))$ should always be bounded. Consequently, the inequity

$$\|\Delta b_k(X,t)\Delta u_k(u_k(t))\| \le M_k \le \infty \tag{30}$$

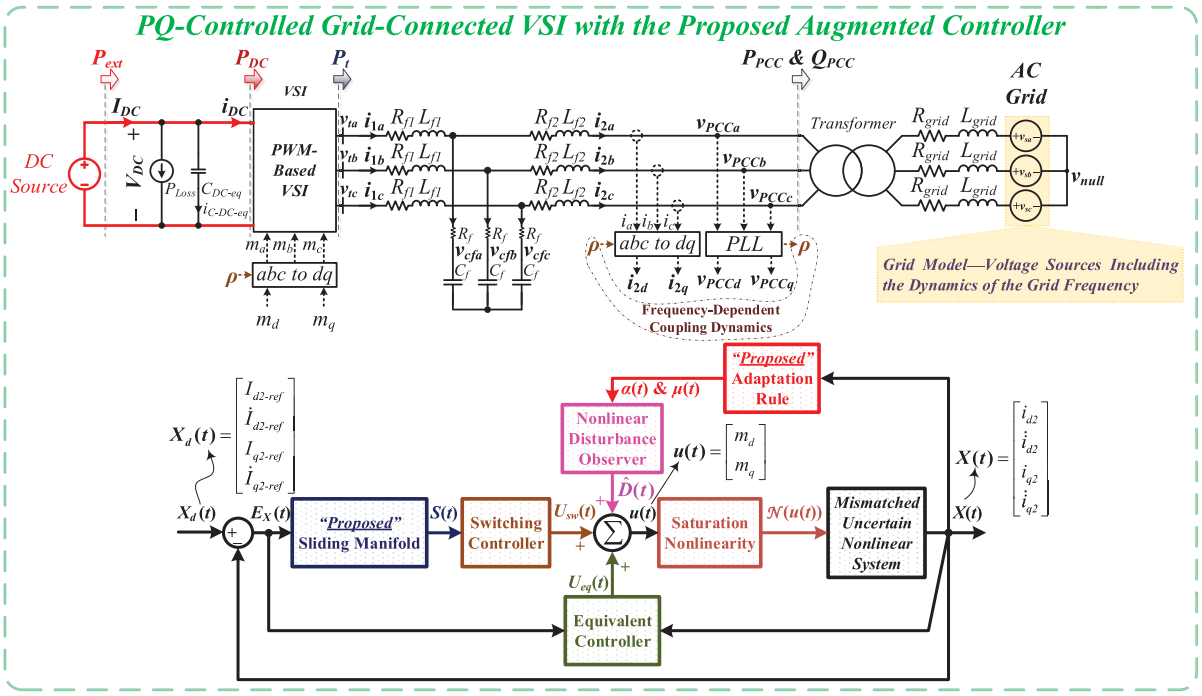

Fig. 3. Schematic of the simulated GC-VSI controlled using the proposed control scheme.

TABLE I
PARAMETERS OF FIG. 3 AND THOSE RELATED TO EXPERIMENTAL SETUP

Parameter	Value
VSC rating of S_n	10.81 kVA
LCL-filter inductance/resistance of L_{f1}/R_{f1}	1.1 mH/0.02 Ω
LCL-filter inductance/resistance of L_{f2}/R_{f2}	1.1 mH/0.02 Ω
LCL-filter's shunt capacitance of C_f/R_f	15.4 μF/2.1 Ω
Switching frequency of f_s	8.1 kHz
DC-side voltage of V_{DC}	400 V
Converter ac-side line-to-line rms low voltage of $V_{PCC_{\text{rms}}}$	208 V
PLL parameters of K_P, K_I, K_D, and K_D's time constant (see Appendix of [7])	180, 3200, 1, and 1×10^{-4}
Inertia constant of H (see Appendix of [10])	1.00 MJ/MVA (for Figs. 4–12)
Governor time constant of τ_g (see Appendix of [10])	0.1 s
Frequency droop coefficient of k_f (see Appendix of [10])	$2S_n/(0.003n_pf_m)$
Damping coefficient of k_p (see Appendix of [10])	8×10^{-5}
Controller parameter of β_k	0.1
Controller parameter of h_k	10^{-12}
Controller parameter of p_k	10^{-12}
Controller parameter of K_k	1000
Controller parameter of η_k	0.001
Controller parameter of $\gamma_{k\text{-}a}$	1000
Controller parameter of $\gamma_{k\text{-}b}$	1000
Controller parameter of $a_{k\text{-}a}$	0.0526
Controller parameter of $a_{k\text{-}b}$	0.1, i.e., $\epsilon = 0.95$ for $k \in \{1, 2\}$

where $k = 1, 2$, and M_k is an unknown positive constant and is required to be satisfied.

Considering the input saturation, the lumped perturbation is accordingly modified as follows:

$$\begin{aligned} D_k(X,u,t) = {} & \Delta f_{2k-1}(X,t) + d_{2k-1}(t) \\ & + \Delta \dot{f}_{2k-1}(X,t) + \dot{d}_{2k-1}(t) \\ & + \Delta f_{2k}(X,t) + d_{2k}(t) \\ & + \Delta b_k(X,t)u_k(t) + \Delta b_k(X,t)\Delta u_k(u_k(t)). \end{aligned} \tag{31}$$

The following assumption is, thus, being made. It is assumed that the lumped perturbation (31) is bounded by unknown parameters $\nu_k \in \mathbb{R}^+$ and $\alpha_k \in \mathbb{R}^+$ as

$$\begin{aligned} \|D_k(X,u,t)\| &\le \alpha_k|\delta_k| + \mu_k + \|b_k(X,t)\|\|\Delta u_k(u_k(t))\| \\ &\le \alpha_k|\delta_k| + \mu_k + M_k \\ &\Rightarrow \|D_k(X,u,t)\| \le \alpha_k|\delta_k| + \nu_k \end{aligned} \tag{32}$$

where it is supposed that $b_k(X,t)$ is bounded and $\nu_k = \mu_k + M_k$.

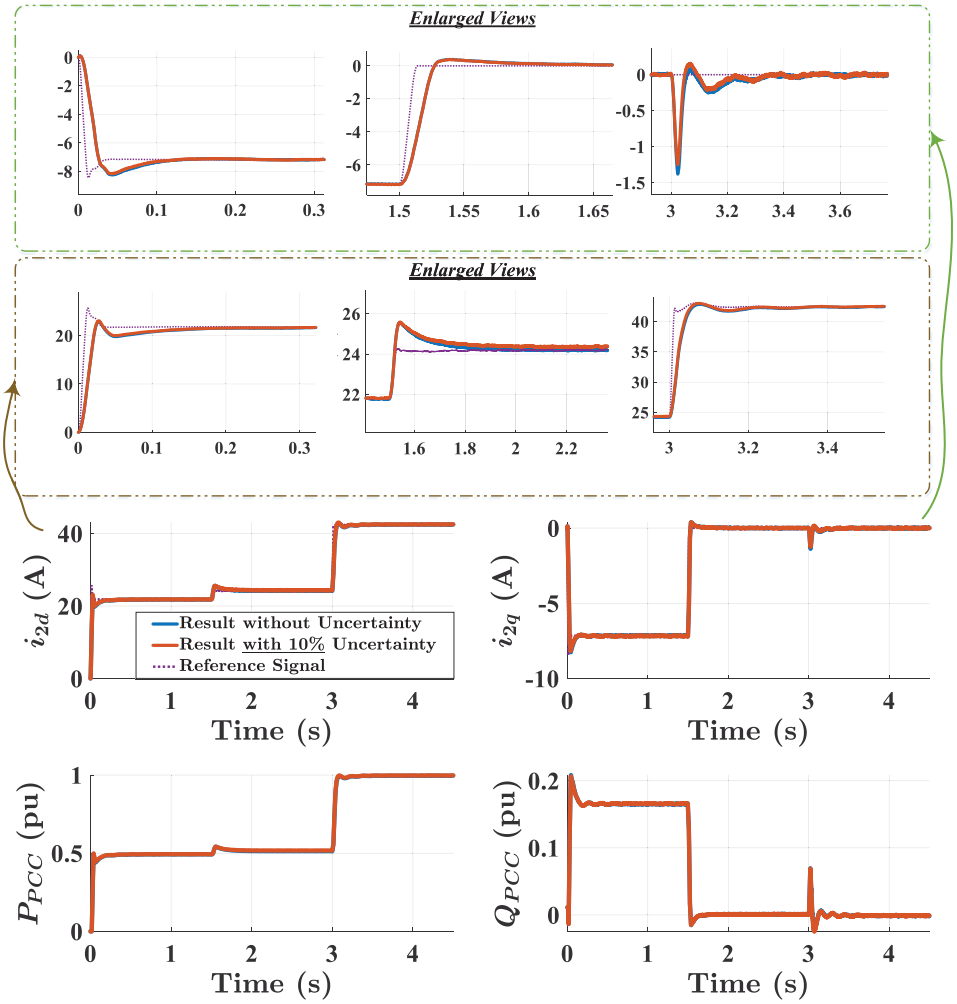

Fig. 4. Test Case I's outcome: simulation results for $SCR = 1$ and $H = 1$—the results without uncertainty (in blue traces), the results with 10% uncertainty in all system parameters (in dark red traces), and the reference signals applied to the system (in violet traces).

Based on *Theorem* 3, it is proven that the following SMC input (33) will reach the designed sliding manifold within a given finite time. Finally, it has proven the stability of the closed-loop system using the proposed sliding manifold

$$u_k(t) = -b_k^{-1}(f_k - \ddot{x}_{d2k-1} + e_{2k} + x_{d2k} - \dot{x}_{d2k-1} + \hat{D}_k + \gamma_{k\text{-}a}\text{sign}(s_{2k-1})|s_{2k-1}|^{a_{k\text{-}a}} + \gamma_{k\text{-}b}\text{sign}(\dot{s}_{2k-1})|\dot{s}_{2k-1}|^{a_{k\text{-}b}} + K_k\text{sign}(\xi_k)) \tag{33}$$

where $k = 1, 2$, $\xi_k = s_{2k} - \delta_k$, K_k is a positive constant, which is the switching gain, and according to (14), $\gamma_{k\text{-}a} > 0$, $\gamma_{k\text{-}b} > 0$, $a_{k\text{-}a} = (a_{k\text{-}b})/(2 - a_{k\text{-}b})$, $a_{k\text{-}b} \in (1 - \epsilon, 1)$, and $\epsilon \in (0, 1)$.

Theorem 3 (Rigorous Stability of the Disturbance Observer—With the Designed Adaptation Rule—Merged With SMC Modular Methodology Using the Proposed Sliding Manifold): Provided that (7) is controlled by the control signal (33) with the saturation of $\mathcal{N}_k(.)$ and combined with the observer (18)—as shown in Fig. 2—then the error states will reach the sliding manifold $s_{2k} = 0$ during a given finite time.

Proof: If the auxiliary variable of ξ_k is defined in (33), a Lyapunov function candidate can be chosen as $V_k^c(t) = 0.5\xi_k^2$. Then, the time derivative of $V_k^c(t)$ becomes

$$\dot{V}_k^c(t) = \xi_k\dot{\xi}_k = \xi_k(\dot{s}_{2k} - \dot{\delta}_k). \tag{34}$$

After a mathematical manipulation, $\dot{s}_{2k} = \ddot{s}_{2k-1} + \gamma_{k\text{-}a}\text{sign}(s_{2k-1})|s_{2k-1}|^{a_{k\text{-}a}} + \gamma_{k\text{-}b}\text{sign}(\dot{s}_{2k-1})|\dot{s}_{2k-1}|^{a_{k\text{-}b}}$; substituting the aforementioned formula associated with $\dot{s}_{2k}$ into (34) above, (35) is found—considering $\ddot{s}_{2k-1} = \ddot{e}_{2k-1} + \dot{e}_{2k-1}$. The last expression is calculated from the first line of (9) and $\ddot{e}_{2k-1} + \dot{e}_{2k-1} = f_k + b_k u_k - \ddot{x}_{d2k-1} + e_{2k} + x_{d2k} - \dot{x}_{d2k-1} + \hat{D}_k = \ddot{s}_{2k-1}$, where b_k has been defined in (4)

$$\begin{aligned}\dot{V}_k^c(t) &= \xi_k(\dot{s}_{2k} - \dot{\delta}_k) \\ &= \xi_k(f_k + b_k u_k - \ddot{x}_{d2k-1} + e_{2k} + x_{d2k} \\ &\quad - \dot{x}_{d2k-1} + \hat{D}_k + \gamma_{k\text{-}a}\text{sign}(s_{2k-1})|s_{2k-1}|^{a_{k\text{-}a}} \\ &\quad + \gamma_{k\text{-}b}\text{sign}(\dot{s}_{2k-1})|\dot{s}_{2k-1}|^{a_{k\text{-}b}}).\end{aligned} \tag{35}$$

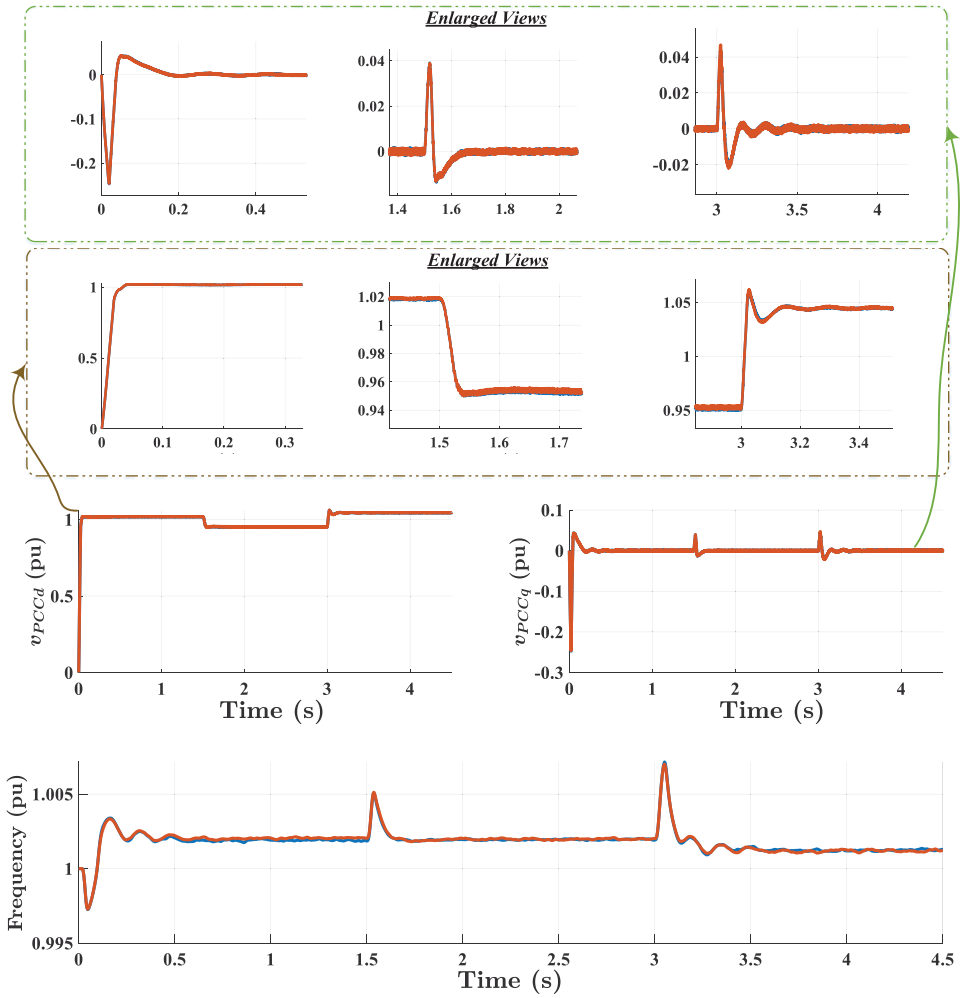

Fig. 5. Test Case I's outcome: disturbance signals impacting the simulated GC-VSI in Fig. 4—the results without uncertainty (in blue traces) and the results with 10% uncertainty in all system parameters (in dark red traces).

Now, when substituting u_k in (35) by the first line of (33), (36) is simply obtained

$$\begin{aligned}\dot{V}_k^c(t) = \xi_k(f_k + b_k[-b_k^{-1}(f_k - \ddot{x}_{d2k-1} + e_{2k} + x_{d2k} \\ - \dot{x}_{d2k-1} + \hat{D}_k + \gamma_{k\text{-}a}\text{sign}(s_{2k-1})|s_{2k-1}|^{a_{k\text{-}a}} \\ + \gamma_{k\text{-}b}\text{sign}(\dot{s}_{2k-1})|\dot{s}_{2k-1}|^{a_{k\text{-}b}} + K_k\text{sign}(\xi_k))] \\ - \ddot{x}_{d2k-1} + e_{2k} + x_{d2k} - \dot{x}_{d2k-1} \\ + \gamma_{k\text{-}a}\text{sign}(s_{2k-1})|s_{2k-1}|^{a_{k\text{-}a}} \\ + \gamma_{k\text{-}b}\text{sign}(\dot{s}_{2k-1})|\dot{s}_{2k-1}|^{a_{k\text{-}b}} + \hat{D}_k) \Longrightarrow \\ \dot{V}_k^c(t) = -\xi_k(K_k\text{sign}(\xi_k)) = -K_k|\xi_k| \leq 0. \end{aligned} \tag{36}$$

Therefore, it is concluded that here $\xi_k = s_{2k} - \delta_{2k} = 0$ is satisfied for $t_k^r \leq (|\xi_k(0)|/K_k) \Rightarrow t_k^r \leq ((|s_{2k}(0) - \delta_k(0)|)/K_k)$. Furthermore, $\delta_k(t) = 0$ is guaranteed according to Theorem 2. Consequently, the condition $s_{2k}(t) = 0$ is also met and the error states will again attain the sliding manifold $s_{2k}(t) = 0$ within the finite time of t_k^r. □

Remark 4: Provided that the control signal (33) controls the tracking error's dynamics of (7) with the saturation function $\mathcal{N}_k(.)$ [given by (26)]—along with the disturbance observer (18)—then the error states will achieve the sliding manifold $s_{2k}(t) = 0$ within a given finite time. Thus, the proof is fully accomplished considering the input saturation function $\mathcal{N}_k(.)$.

Remark 5: It is noteworthy that, as previously proven through Theorems 2 and 3, any constants $\beta_k > 0$, $h_k > 0$, $K_k > 0$, $\eta_k > 0$, $\gamma_{k\text{-}a} > 0$, $\gamma_{k\text{-}b} > 0$, $a_{k\text{-}a} = (a_{k\text{-}b}/(2 - a_{k\text{-}b}))$, $a_{k\text{-}b} \in (1 - \epsilon, 1)$ with $\epsilon \in (0, 1)$ satisfy the Lyapunov stability criteria. The time response of the dynamic system from the standpoint of the transient performance is able to help the designer select the most appropriate value for the constants above. In other words, this work has not focused on choosing the "optimal" amount of them systematically as it is out of the scope of this research. This article has also proved that the global stability of the closed-loop system with the proposed control is rigorously guaranteed. However, it does not make any comments on robust performance at all.

IV. Simulation Results

This section elaborates on the simulation results. The first subsection provides the simulations associated with the proposed controller. Sections IV-B and IV-C detail the comparative simulations; the controllers employed in comparisons

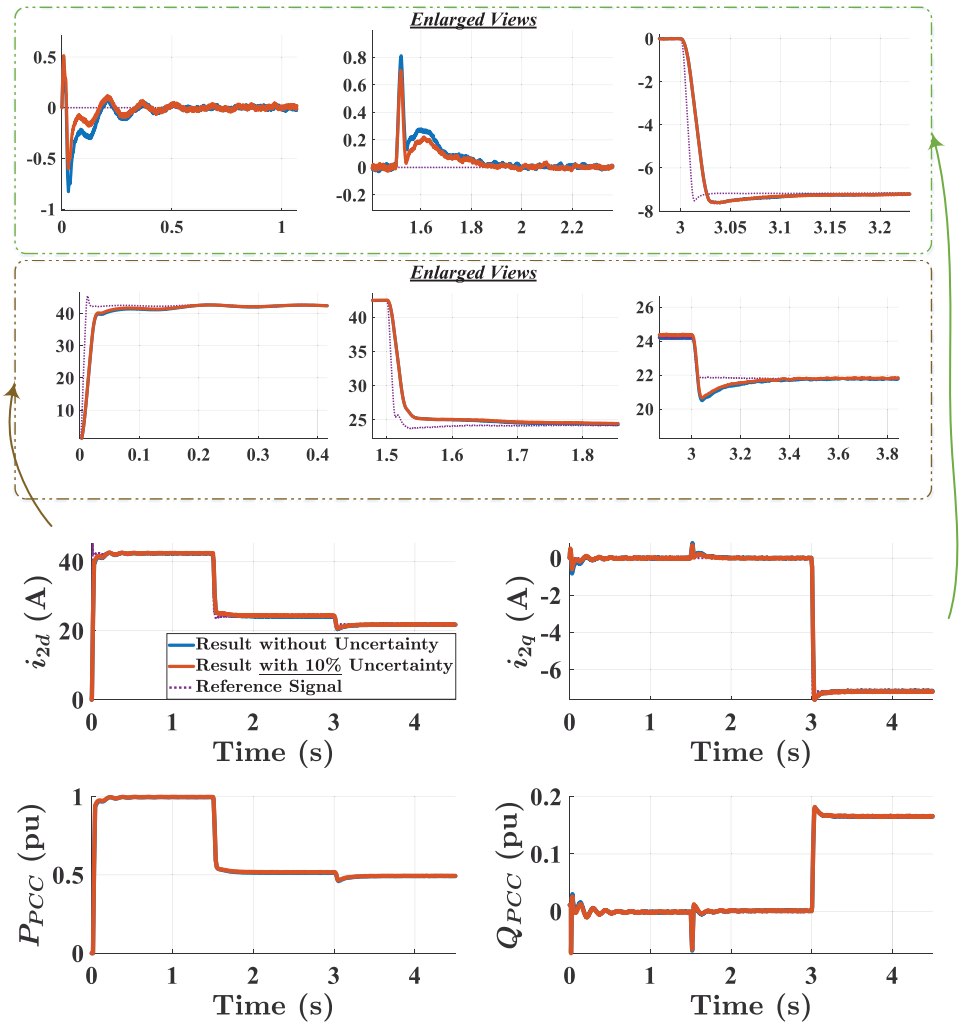

Fig. 6. Test Case II's outcome: simulation results for $SCR = 1$ and $H = 1$—the results without uncertainty (in blue traces), the results with 10% uncertainty in all system parameters (in dark red traces), and the reference signals applied to the system (in violet traces).

are a robust sliding-mode controller—with a "single-integral" sliding surface and without adaptive disturbance observer—and the PI controller, which is an industrially acceptable one, respectively.

A. Simulation Results of the Proposed Controller

Fig. 3 with the parameters given in Table I has been simulated using the Simulink in MATLAB as a GC-VSI—whose frequency-dependent ac grid has been simulated via the model in [10, Appendix]. The detailed switching model of the VSC is used in the simulation for better accuracy. Thus, the control performance of the VSC under typical high-frequency disturbances of switching-based loads and the low-frequency ones caused by the PLL and the ac grid's frequency dynamics is examined. It is noteworthy that all parameters have been selected to examine the proposed 2DoF modular controller as harshly as possible, and they are still close to the practical cases. As regards this consideration, for the simulated grid shown in Fig. 3, the lowest possible value of the equivalent moment of inertia of J (or comparably inertia constant of H) and control gains associated with the governors has been selected to be simulated here. Moreover, the lowest available short-circuit capacity ratio (SCCR) has been chosen so that the most potentially practical disturbance dynamics are made as per studies [6], [7].

Moreover, the parameters of the PLL's PID controller employed have also been reported and detailed in Table I. It is able to produce an almost 90° phase margin with the adequate bandwidth for the PLL dynamics. As the PLL controller is a simple PID inducing a 90° phase margin with enough bandwidth, a low-inertia grid—whose frequency significantly fluctuates—impacts the PLL performance. Consequently, it creates a practically functional disturbance associated with frequency changes on the closed-loop system of the GC-VSI. It is able to produce an almost 90° phase margin with adequate bandwidth for the PLL dynamics. As the PLL controller is a simple PID inducing a 90° phase margin with enough bandwidth, a low-inertia grid—whose frequency fluctuates significantly—impacts the PLL performance.

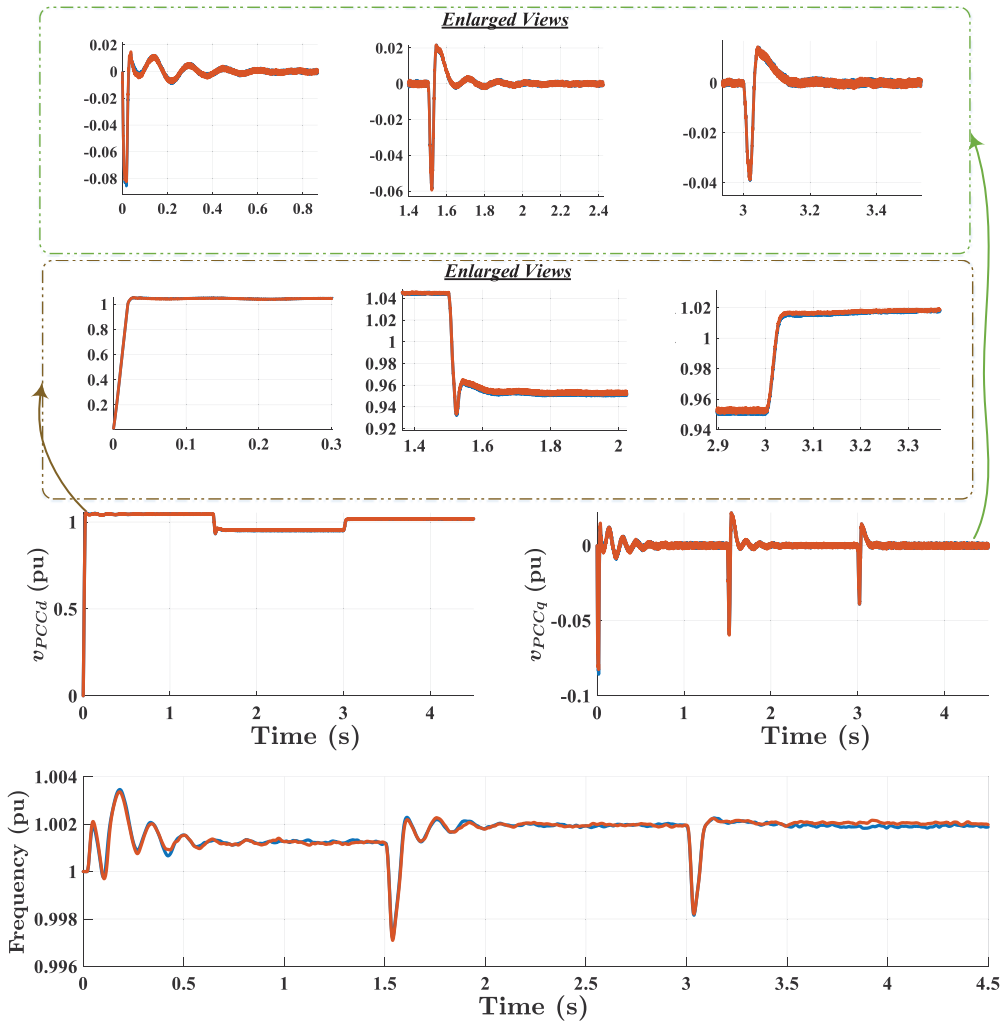

Fig. 7. Test Case II's outcome: disturbance signals impacting the simulated GC-VSI in Fig. 6—the results without uncertainty (in blue traces) and the results with 10% uncertainty in all system parameters (in dark red traces).

Consequently, it creates the worst practically functional disturbance associated with frequency changes on the closed-loop system of the GC-VSI.

All controllers used in the frequency regulation and the PLL have the industrially accepted structure and parameters. Moreover, the system—with and without 10% uncertainty in all parameters—has been simulated and examined under various low-inertia and weak grid conditions. Additionally, various reference signals have been generated—with and without arbitrary shapes—in order to test the effectiveness of the controller proposed during both transient and steady-state responses. Figs. 4–7 show the aforementioned simulations demonstrating i_{2d} in (A), i_{2q} in (A), and active/reactive power in per unit (pu)—where the results of the system without uncertainty are shown by traces in blue, and the results of the system with 10% uncertainty are shown by traces in dark red, and the applied reference signals are shown by traces in violet.

In order to adequately assess the effectiveness of the proposed controller, two general test cases have been selected to be simulated. One examines a significant change in the reactive power, and the other evaluates a high variation in the active power at the beginning of simulations, as elaborated in the following.

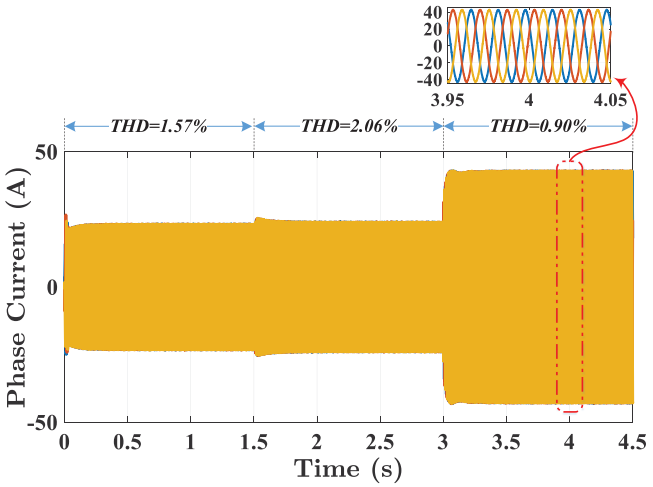

Fig. 8. THD of the PCC current associated with Test Case I (in Fig. 4), which is controlled by the proposed controller.

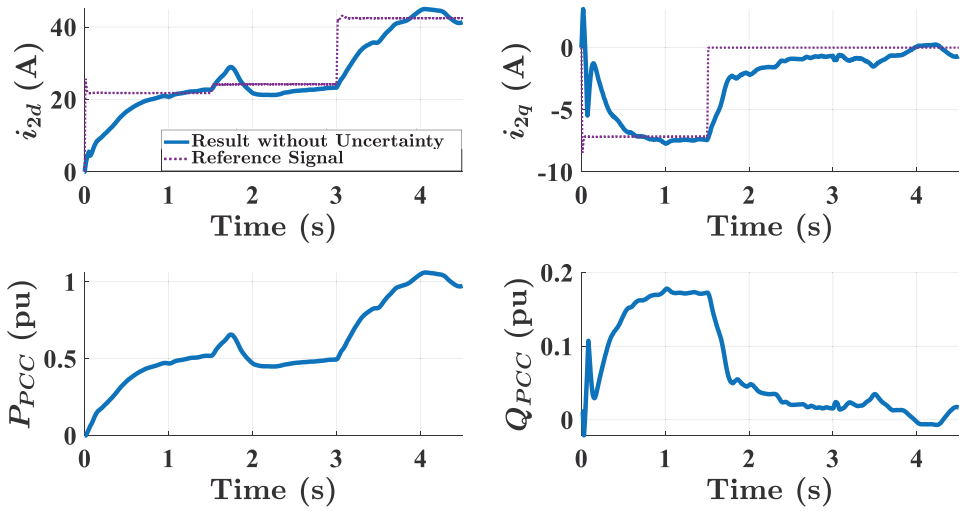

Fig. 9. Test Case I's outcome: Fig. 4's counterpart simulation results for $SCR = 1$ and $H = 1$, using a robust controller without adaptive disturbance observer.

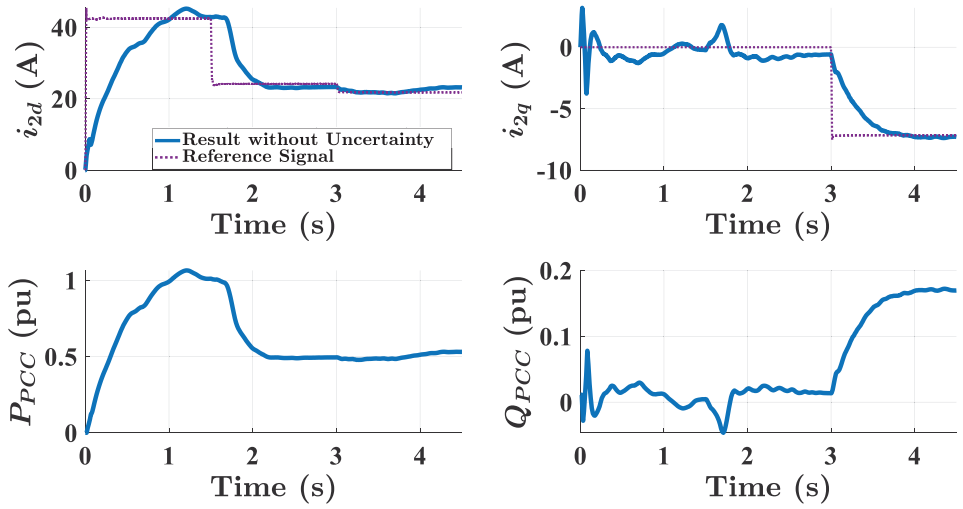

Fig. 10. Test Case II's outcome: Fig. 6's counterpart simulation results for $SCR = 1$ and $H = 1$, using a robust controller without adaptive disturbance observer.

Test Case I: Test Case I deals with high reactive power variation and low active power variation at the beginning. Then, in this test case, the power factor (PF) is changed from 0.95 to 1.0 at $t = 1.5$ s, and the active power is varied from 0.5 pu to 1.00 pu at $t = 3.0$ s. Fig. 4 demonstrates the results of Test Case I. The rest of the changes in the references of i_{2d} and i_{2q} (and their according effects on active/reactive power) has been shown in Fig. 4 for the worst case of grid conditions—i.e., SCCR equals to 1 and $H = 1$ [6]. Fig. 4 and its various enlarged views associated with different changes show the proposed 2DoF controller's capability to stabilize i_{2d} and i_{2q}, and their performances are very satisfactory. Fig. 5 shows the related disturbance signals (including $\upsilon_{\mathrm{PCC}d}$, $\upsilon_{\mathrm{PCC}q}$, and frequency all in pu) associated with our simulations results in Fig. 4.

Test Case II: Test Case II deals with high active power variation and low reactive power variation at the beginning. Then, in this test case the active power is varied from 1.0 pu to 0.5 pu at $t = 1.5$ s, and the PF is changed from 1.0 to 0.95 at $t = 3.0$ s—again for SCCR $= 1$ and $H = 1$. Fig. 6 shows the results of Test Case II. Fig. 6 and its various enlarged views associated with different changes show the proposed 2DoF controller's capability of stabilizing i_{2d} and i_{2q} very satisfactorily again. Fig. 7 reveals the related disturbance signals associated with our simulations shown in Fig. 6.

Finally, as the power quality of the current converter matters—and it will be impacted by both control and switching strategy—the total harmonic distortion (THD) of the current waveform has been reported and demonstrated in Fig. 8. It shows the THD of the PCC current during various active/reactive power changes associated with Test Case I, for example. As shown in Fig. 8, it is within the recommended limits detailed in the IEEE Standard 519, i.e., less than 2.5%, which is the limit for the V_{PCC} up to 161 kV [34].

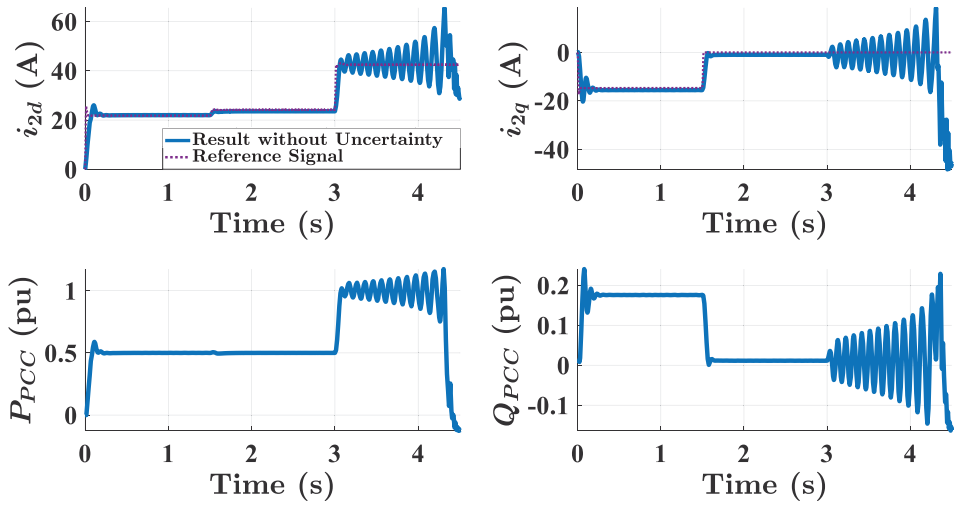

Fig. 11. Test Case I's outcome: Fig. 4's counterpart simulation results for $SCR = 1$ and $H = 1$, using a PI controller without adaptive disturbance observer.

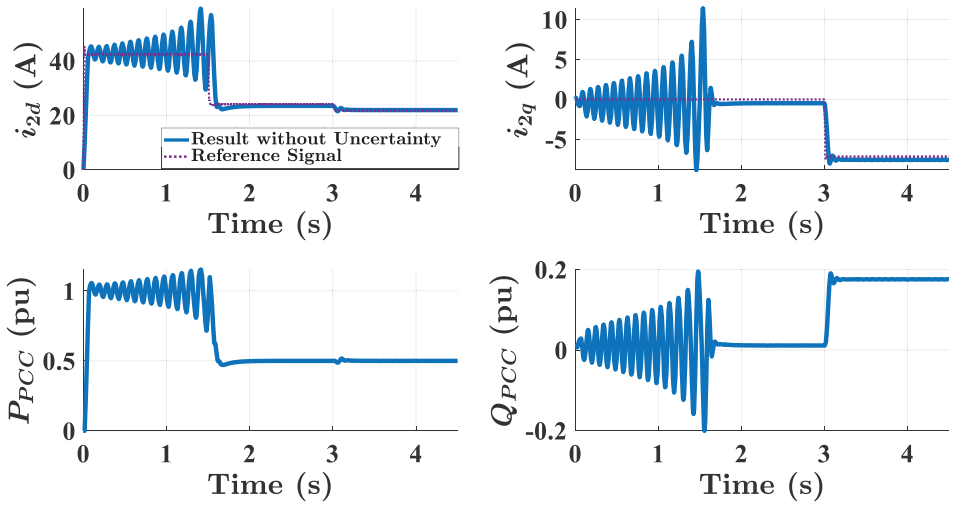

Fig. 12. Test Case II's outcome: Fig. 6's counterpart simulation results for $SCR = 1$ and $H = 1$, using a PI controller without adaptive disturbance observer.

B. Simulation Results of the Single-Integral Robust SMC Without an Adaptive Disturbance Observer

In this section, another robust controller using a single-integral sliding surface without an adaptive disturbance observer is proposed for comparison. It has been synthesized as follows.

A single-fold sliding mode controller, whose surface has been detailed in the following, is designed as:

$$s_{2k}(t) = e_{2k}(t) + \int_0^t (k_1 e_{2k}(\tau) + k_2 e_{2k-1}(\tau))d\tau \quad (37)$$

in which k_1 and k_2 are constant positive real numbers.

For the case without mismatched uncertainty, the dynamics of $\dot{s}(t)$ is found as

$$\dot{s}_{2k}(t) = 0 \Rightarrow \dot{e}_{2k} = -(k_1 e_{2k}(t) + k_2 e_{2k-1}(t)). \quad (38)$$

Therefore

$$\begin{cases} \dot{e}_{2k-1}(t) = e_{2k}(t), \\ \dot{e}_{2k}(t) = f_k(X,t) - \dot{x}_{d2k}(t) + \Delta f_{2k}(X,t) + d_{2k}(t) \\ \qquad + [b_k(X,t) + \Delta b_k(X,t)]\mathcal{N}_k(u_k(t)). \end{cases} \quad (39)$$

Considering (39) and defining the lumped uncertainty of $\Delta L_{2k}(t)$ as

$$\Delta L_{2k}(t) \triangleq -\Delta f_{2k}(X,t) + d_{2k}(t) + \Delta b_k(X,t)\mathcal{N}_k(u_k(t)) + b_k(X,t)\Delta u_k(u_k(t)) \quad (40)$$

results in

$$\begin{cases} \dot{e}_{2k-1}(t) = e_{2k}(t) \\ \dot{e}_{2k}(t) = f_k(X,t) - \dot{x}_{d2k}(t) + b_k(X,t)\mathcal{N}_k(u_k(t)) \\ \qquad + \Delta L_{2k}(t). \end{cases} \quad (41)$$

Therefore, assuming $\|\Delta L_{2k}(t)\| \leq \Omega_{2k}$, in which Ω_{2k} is a large enough constant number, causes

$$u_k(t) = -b_k^{-1}(f_k(X,t) + \dot{x}_{2k}(t) - k_1 e_{2k}(t) - k_2 e_{2k-1}(t) - K\,\mathrm{sign}(s_{2k}(t))) \quad (42)$$

where $K > \Omega_{2k}$.

It is noteworthy that in deriving (42), it is assumed that there exists only a single sliding surface and that Ω_{2k} is a large enough "constant" number. It means that although a robust controller is synthesized, first, a single-integral sliding

surface exists, and second, there is not any adaptive disturbance observer in the structure—as shown in Fig. 2. The aforementioned points are in direct contrast to the proposed controller.

Now, by inserting (38) into the system dynamics of (7), the sliding mode dynamics can be found as

$$\begin{cases} \dot{e}_{2k-1}(t) = e_{2k}(t) \\ \dot{e}_{2k}(t) = -k_1 e_{2k}(t) - k_2 e_{2k-1}(t). \end{cases} \tag{43}$$

It is clear that (43) is stable provided that k_1 and k_2 are suitable constant positive real numbers.

Theorem 4 (Finite-Time Stability of the Reaching Phase of the Robust Single-Integral SMC): The states of the stable equilibrium point of the system (41) with the controller (42) will converge o the sliding surface $s_{2k}(t) = 0$ in a given finite time—if $K > \Omega_{2k}$.

Proof: By defining $V_{2k}^d(t) = 0.5e_{2k}^2(t)$ as a candidate for the Lyapunov function—required for the combination of (37) and (39)–(42) —the following expression for $\dot{V}_{2k}^d(t)$ is achieved:

$$\begin{aligned} \dot{V}_{2k}^d(t) &= s_{2k}(t)\dot{s}_{2k}(t) \\ &= s_{2k}(t)(\dot{e}_{2k}(t) + k_1 e_{2k}(t) + k_2 e_{2k-1}(t)). \end{aligned} \tag{44}$$

Using (7) results in

$$\begin{aligned} \dot{V}_{2k}^d(t) = s_{2k}(t)(&f_k(X,t) - \dot{x}_{d2k}(t) + \Delta f_{2k}(X,t) + d_{2k}(t) \\ &+ [b_k(X,t) + \Delta b_k(X,t)]\mathcal{N}_k(u_k(t)) \\ &+ k_1 e_{2k}(t) + k_2 e_{2k-1}(t)). \end{aligned} \tag{45}$$

Combing (40), (45), and (42), and benefiting from $s_{2k}(t)\text{sign}(s_{2k}(t)) = |s_{2k}(t)|$ and $K > \Omega_{2k}$, $\dot{V}_{2k}^d(t)$ is calculated as

$$\dot{V}_{2k}^d(t) \leq (-K + \Omega_{2k})|s_{2k}(t)| \leq 0. \tag{46}$$

Therefore, writing $t_{2k}^r \leq (|s_{2k}(0)|)/(K - \Omega_{2k})$, $s_{2k}(t) = 0$ is guaranteed, which completes and concludes the proof. □

Figs. 9 and 10 show the counterparts of Figs. 4 and 6 while the robust controller (42) is being used. As demonstrated, the performance of the proposed controller is much better than that of the robust controller of (42)—albeit a robust controller—from the perspective of time response, i.e., settling time, rise time, time constant, and under/overshoot.

C. Simulation Results of the PI Controller

In this section, the industrially accepted controller has been employed. The synthesized controller (with $k_p = 2.2$ and $k_i = 40$) makes a 1-ms time constant for the active/and reactive power controls. This PI controller is very well known in the literature [12], [35]. It has been shown that PI controller shows instability for the $SCCR = 1$ in many studies (see [6], [7], and references therein). The parameters of the PLL PID controller employed have been reported and detailed in Table I. It is able to produce an almost 90° phase margin with adequate bandwidth for the PLL dynamics. As the PLL controller is a simple PID inducing a 90° phase margin with enough bandwidth, a low-inertia grid—whose frequency fluctuates significantly—impacts the PLL performance. Consequently, it creates a practically functional disturbance associated with frequency changes on the closed-loop system of the GC-VSI.

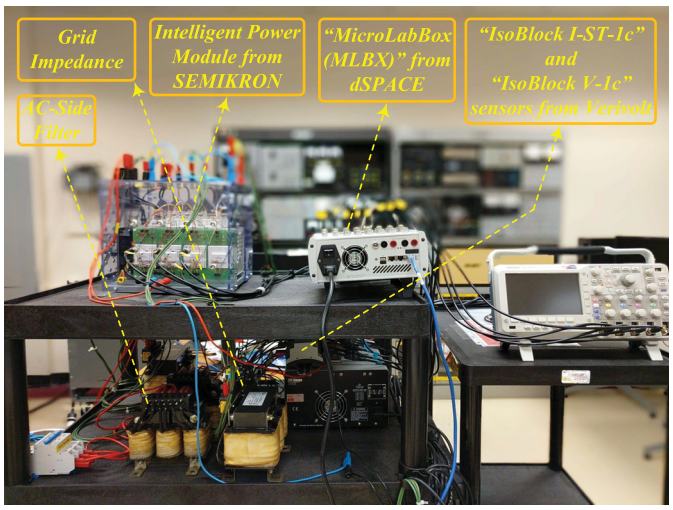

Fig. 13. Photograph of the scaled-down test rig for conducting experiments.

Figs. 11 and 12 show the counterparts of Figs. 4 and 6 while the PI controller elaborated earlier is being used. As shown, the performance of the proposed controller is much better than that of the robust single-integral SMC of (42)—and the PI controller is even unstable in the full power of $P = 1$ and $Q = 0$. This instability is widespread in two-level VSIs controlled by a PI controller, which has been reported in several research works (see [6], [7], and references therein). One of the main reasons for this instability is that the nonlinear dynamics of the PLL are highly coupled in low SCCRs, and therefore, a simple PI controller cannot remove its impacts. In the proposed controller, however, the PLL dynamics (as disturbance signals) are observed and supplied via feedforward signals shown in Fig. 3.

V. Experimental Results

For further evaluation of the proposed controller, an experimental test rig is employed to examine the performance of the GC-VSI equipped with an LC-filter in the dc side and with an LCL-filter on the ac side of the test rig. The experimental system consists of a GC-VSI, operating as an inverter (i.e., dc to ac power conversion), regularly and frequently operating in the FIPES' MIACDC power systems. The VSI is controlled like what has been done for the simulation results in Section IV, which yields the operating conditions with respect to the ac-side dynamics. An intelligent power module from *SEMIKRON*—which includes six insulated gate bipolar transistors (IGBTs) built by three "*SKM 50 GB 123 D*" modules, three "*SKHI 21A (R)*" gate drives, and protection circuits—is used in order to implement the power electronic converter needed. The experimental setup's parameters—which are the same as the simulated circuit's parameters—and controller values have been reported in Table I.

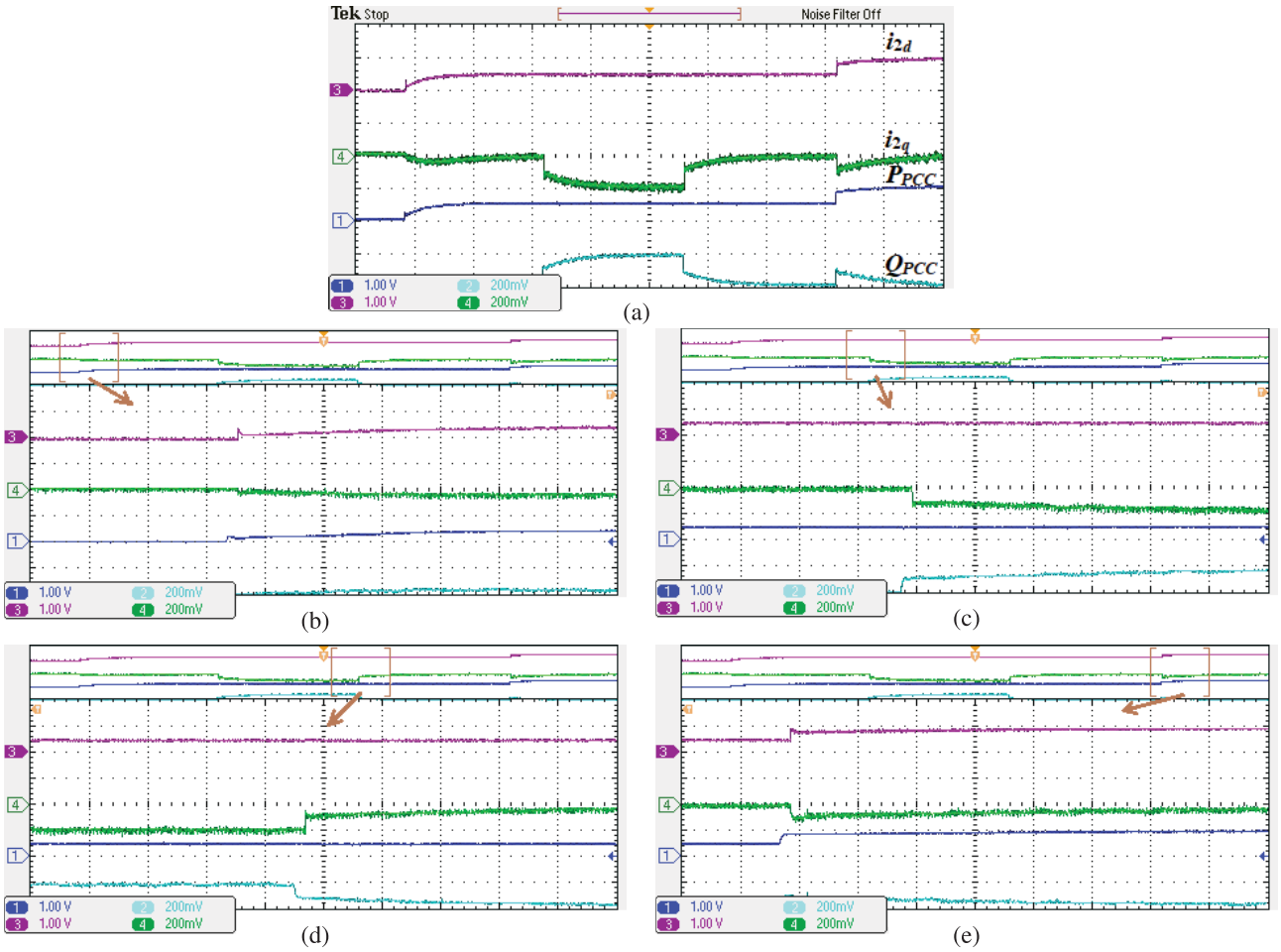

Fig. 14. Test Case I's outcome: experimental results (associated with simulations in Fig. 4). (a) Whole picture (500 ms/div) and (b)–(e) enlarged view of different parts (100 ms/div), showing P_{PCC} via Channel 1 (in dark blue) with 10.80 kW/div, Q_{PCC} via Channel 2 (in cyan) with 2.16 kvar/div, i_{2d} via Channel 3 (in dark magenta) with 42.43 A/div, and i_{2q} via Channel 4 (in law green) with 8.49 A/div—V/div of each channel has been shown at the left-bottom corner for all variables in pu.

The VSI's inductor currents and voltages are measured by "*IsoBlock I-ST-1c*" current sensors and "*IsoBlock V-1c*" voltage sensors from "*Verivolt*," respectively. The converter is interfaced with a MicroLabBox (MLBX) from "*dSPACE*." The proposed control algorithm is executed and run by a dual-core, 2 GHz "*NXP (Freescale) QorlQ P5020*" real-time processor. The PWM signals are generated by "*Xilinx Kintex-7 XC7K325T*" field-programmable gate arrays (FPGAs) connected to digital inputs/outputs (I/Os). The MLBX interface board is equipped with eight 14-b, 10-megasample-per-second, differential analog-to-digital channels to interface the measured signals to the control system (with the functionality of free-running mode). The software code is generated by the real-time-workshop under the MATLAB/Simulink environment. Fig. 13 shows a snapshot of the test rig used.

In order to be able to compare the simulations with experiments, the same Test Cases I and II elaborated in Section IV-A have been employed here. Figs. 14 and 15 have shown the outcomes of the experiments conducted. The same experiments as what has been simulated through Test Cases I and II (i.e., Figs. 4 and 6, respectively) have been done with the test rig mentioned earlier. In Figs. 14 and 15, i_{2d}, i_{2q}, P, and Q (all in pu) have been shown by traces in magenta, green, blue, and cyan, respectively—whose values associated with the volts-per-division (V/div) have been noted at the left-bottom corner of Figs. 14 and 15 as well. Figs. 14 and 15 show that the control algorithm is implementable and able to effectively stabilize the active power and reactive power of the GC-VSI under test.

It is noteworthy that in our experiments, based on the available resources and devices' capabilities, there has been a power plug supplied by the university's utility grid without any possibility to model a network with low inertia. In other words, our grid model is equivalent to a Thevenin's circuit, whose inertia is high and thus having an almost fixed frequency. More importantly, there are always some practical uncertainties (which are common) in any experiments compared to simulations, especially when dealing with creating weak-grid conditions. According to the reasoning mentioned earlier, it is impossible to exactly replicate some test cases gained from simulation results by means of the available test rig. Having said that, this section has shown that the proposed control

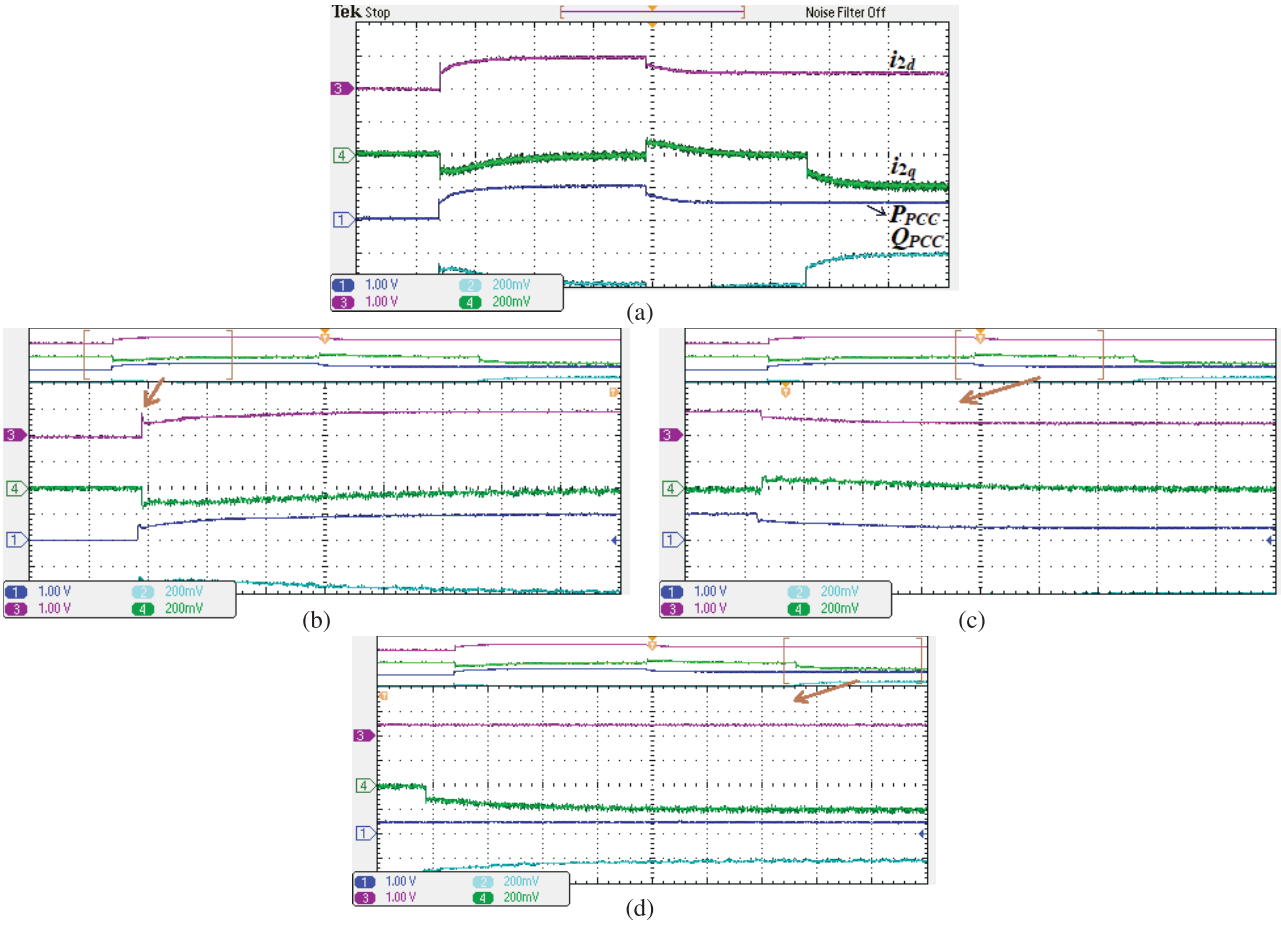

Fig. 15. Test Case II's outcome: experimental results (associated with simulations in Fig. 6). (a) Whole picture (500 ms/div) and (b)–(d) enlarged view of different parts (100 ms/div)—showing $P_{\rm PCC}$ via Channel 1 (in dark blue) with 10.80 kW/div, $Q_{\rm PCC}$ via Channel 2 (in cyan) with 2.16 kvar/div, i_{2d} via Channel 3 (in dark magenta) with 42.43 A/div, and i_{2q} via Channel 4 (in law green) with 8.49 A/div—V/div of each channel has been shown at the left-bottom corner for all variables in pu.

scheme is implementable and has shown the effectiveness of the controller—based on the devices' capabilities and resources available to us.

VI. Conclusion

This article has proposed a novel 2DoF modular control approach to better control both active and reactive power of GC-VSIs to be able to be integrated into the emerging multiterminal ac/dc grids. This article has proposed a mathematical model and an innovative control methodology based on the GC-VSI's dynamics in the dq-frame. The synthesized controller is able to improve the stability of GC-VSIs for emerging grid conditions with frequency-dependent dynamics. Those dynamics are tailored to the weak grids, whose inertia may be small and which impact the PLL's dynamics. Also, there are uncertainties associated with the parameters in the system under study—thus dealing with mismatched disturbances and uncertainties. From the standpoint of control theories, overcoming mismatched disturbances and uncertainties is a difficult task in control of nonlinear systems due to the absence of a direct control signal for the affected states. For solving this problem, a new enhanced control structure, which is modular, has been offered. It has employed the well-known sliding-mode control (with a new sliding manifold) combined with a disturbance observer (with a new adaptation rule) that has been introduced. The introduced control guarantees that the effects of mismatched uncertainties, external disturbances, and control fluctuations (with completely unknown bounds) are successfully canceled without any steady-state errors. Comprehensive mathematical analysis, simulations, and experiments have been provided in order to show the effectiveness of the recommended methodology.

Acknowledgment

The authors would like to thank SEMIKRON Company (https://www.semikron.com/), Verivolt Company (https://www.verivolt.com), and dSPACE GmbH Company (https://www.dspace.com/en/inc/home/products/hw/microlabbox.cfm) for kindly providing Georgia Southern University with partial support.

References

[1] U. S. Department of Energy. (Nov. 2014). *The War Currents: AC vs. DC Power*. [Online]. Available: http://energy.gov/articles/war-currents-ac-vs-dc-power

[2] *IEEE Standard for Interconnection and Interoperability of Distributed Energy Resources With Associated Electric Power Systems Interfaces*, IEEE Standard 1547-2018, Apr. 2018, doi: 10.1109/IEEESTD.2018.8332112.

[3] R. Das, V. Madani, and A. P. S. Meliopoulos, "Leveraging smart grid technology and using microgrid as a vehicle to benefit DER integration," in *Proc. IEEE Power Energy Soc. Innov. Smart Grid Technol. Conf. (ISGT)*, Apr. 2017, pp. 1–5.

[4] J. Shiles *et al.*, "Microgrid protection: An overview of protection strategies in north American microgrid projects," in *Proc. IEEE Power Energy Soc. Gen. Meeting*, Jul. 2017, pp. 1–5.

[5] I. U. Nutkani *et al.*, "Autonomous power management for interlinked AC-DC microgrids," *CSEE J. Power Energy Syst.*, vol. 4, no. 1, pp. 11–18, Mar. 2018.

[6] M. Davari and Y. A.-R.-I. Mohamed, "Robust vector control of a very weak-grid-connected voltage-source converter considering the phase-locked loop dynamics," *IEEE Trans. Power Electron.*, vol. 32, no. 2, pp. 977–994, Feb. 2017.

[7] A. Aghazadeh, M. Davari, H. Nafisi, and F. Blaabjerg, "Grid integration of a dual two-level voltage-source inverter considering grid impedance and phase-locked loop," *IEEE J. Emerg. Sel. Topics Power Electron.*, early access, Nov. 14, 2019, doi: 10.1109/JESTPE.2019.2953522.

[8] M. Karimi-Ghartemani and M. R. Iravani, "A method for synchronization of power electronic converters in polluted and variable-frequency environments," *IEEE Trans. Power Syst.*, vol. 19, no. 3, pp. 1263–1270, Aug. 2004.

[9] M. Karimi-Ghartemani, *Enhanced Phase-Locked Loop Structure for Power Energy Application*. Hoboken, NJ, USA: Wiley, 2014.

[10] S. Silwal, S. Taghizadeh, M. Karimi-Ghartemani, M. J. Hossain, and M. Davari, "An enhanced control system for single-phase inverters interfaced with weak and distorted grids," *IEEE Trans. Power Electron.*, vol. 34, no. 12, pp. 12538–12551, Dec. 2019. [Online]. Available: https://ieeexplore.ieee.org/abstract/document/8682131

[11] M. P. Kazmierkowski and L. Malesani, "Current control techniques for three-phase voltage-source PWM converters: A survey," *IEEE Trans. Ind. Electron.*, vol. 45, no. 5, pp. 691–703, Oct. 1998.

[12] A. Yazdani and R. Iravani, *Voltage-Sourced Converters Power Systems: Modeling, Control, Application*. Hoboken, NJ, USA: Wiley, 2010.

[13] B. Bahrani, S. Kenzelmann, and A. Rufer, "Multivariable-PI-based *dq* current control of voltage source converters with superior axis decoupling capability," *IEEE Trans. Ind. Electron.*, vol. 58, no. 7, pp. 3016–3026, Jul. 2011.

[14] A. Egea-Alvarez, S. Fekriasl, F. Hassan, and O. Gomis-Bellmunt, "Advanced vector control for voltage source converters connected to weak grids," *IEEE Trans. Power Syst.*, vol. 30, no. 6, pp. 3072–3081, Nov. 2015.

[15] M. Davari and Y. A.-R.-I. Mohamed, "Dynamics and robust control of a grid-connected VSC in multiterminal DC grids considering the instantaneous power of DC- and AC-side filters and DC grid uncertainty," *IEEE Trans. Power Electron.*, vol. 31, no. 3, pp. 1942–1958, Mar. 2016.

[16] N. Panten, N. Hoffmann, and F. W. Fuchs, "Finite control set model predictive current control for grid-connected voltage-source converters with LCL filters: A study based on different state feedbacks," *IEEE Trans. Power Electron.*, vol. 31, no. 7, pp. 5189–5200, Jul. 2016.

[17] R. N. Beres, X. Wang, M. Liserre, F. Blaabjerg, and C. L. Bak, "A review of passive power filters for three-phase grid-connected voltage-source converters," *IEEE J. Emerg. Sel. Topics Power Electron.*, vol. 4, no. 1, pp. 54–69, Mar. 2016.

[18] L. Harnefors, X. Wang, A. G. Yepes, and F. Blaabjerg, "Passivity-based stability assessment of grid-connected VSCs—An overview," *IEEE J. Emerg. Sel. Topics Power Electron.*, vol. 4, no. 1, pp. 116–125, Mar. 2016.

[19] H. Liu *et al.*, "An enhanced dual droop control scheme for resilient active power sharing among paralleled two-stage converters," *IEEE Trans. Power Electron.*, vol. 32, no. 8, pp. 6091–6104, Aug. 2017.

[20] M. Davari and Y. A.-R.-I. Mohamed, "Robust droop and DC-bus voltage control for effective stabilization and power sharing in VSC multiterminal DC grids," *IEEE Trans. Power Electron.*, vol. 33, no. 5, pp. 4373–4395, May 2018.

[21] A. Ayachit, Y. P. Siwakoti, V. P. N. Galigekere, M. K. Kazimierczuk, and F. Blaabjerg, "Steady-state and small-signal analysis of A-source converter," *IEEE Trans. Power Electron.*, vol. 33, no. 8, pp. 7118–7131, Aug. 2018.

[22] D. Zhou, Y. Song, and F. Blaabjerg, *Control of Power Electronic Converters and Systems*, vol. 1. New York, NY, USA: Academic, 2018, ch. 5, pp. 117–151.

[23] Z. Ali, N. Christofides, L. Hadjidemetriou, E. Kyriakides, Y. Yang, and F. Blaabjerg, "Three-phase phase-locked loop synchronization algorithms for grid-connected renewable energy systems: A review," *Renew. Sustain. Energy Rev.*, vol. 90, pp. 434–452, Jul. 2018.

[24] J. Bitsch, Nørgaard, M. K. Graungaard, T. Dragičević, and F. Blaabjerg, "Current control of LCL-filtered grid-connected vsc using model predictive control with inherent damping," in *Proc. 20th Eur. Conf. Power Electron. Appl. (EPE ECCE Eur.)*, Nov. 2018, pp. 1–11.

[25] M. P. Aghababa, "Sliding-mode control composite with disturbance observer for tracking control of mismatched uncertain nDoF nonlinear systems," *IEEE/ASME Trans. Mechatronics*, vol. 23, no. 1, pp. 482–490, Feb. 2018.

[26] V. I. Utkin, *Sliding Modes in Control and Optimization*. Berlin, Germany: Springer, 2011.

[27] M. Davari and Y. A.-R.-I. Mohamed, "Variable-structure-based nonlinear control for the master VSC in DC-energy-pool multiterminal grids," *IEEE Trans. Power Electron.*, vol. 29, no. 11, pp. 6196–6213, Nov. 2014.

[28] M. H. Choi, B. Shirinzadeh, and R. Porter, "System identification-based sliding mode control for small-scaled autonomous aerial vehicles with unknown aerodynamics derivatives," *IEEE/ASME Trans. Mechatronics*, vol. 21, no. 6, pp. 2944–2952, Dec. 2016.

[29] A. M. Hava, R. J. Kerkman, and T. A. Lipo, "Carrier-based PWM-VSI overmodulation strategies: Analysis, comparison, and design," *IEEE Trans. Power Electron.*, vol. 13, no. 4, pp. 674–689, Jul. 1998.

[30] A. M. Hava, S.-K. Sul, R. J. Kerkman, and T. A. Lipo, "Dynamic overmodulation characteristics of triangle intersection PWM methods," *IEEE Trans. Ind. Appl.*, vol. 35, no. 4, pp. 896–907, Jul. 1999.

[31] A. A. Rockhill, M. Liserre, R. Teodorescu, and P. Rodriguez, "Grid-filter design for a multimegawatt medium-voltage voltage-source inverter," *IEEE Trans. Ind. Electron.*, vol. 58, no. 4, pp. 1205–1217, Apr. 2011.

[32] S. P. Bhat and D. S. Bernstein, "Geometric homogeneity with applications to finite-time stability," *Math. Control, Signals, Syst.*, vol. 17, no. 2, pp. 101–127, Jun. 2005.

[33] H. K. Khalil, *Nonlinear System Theory*, 3rd ed. Upper Saddle River, NJ, USA: Prentice-Hall, 2002.

[34] *IEEE Recommended Practice and Requirements for Harmonic Control in Electric Power Systems*, IEEE Standard 519-2014, Jun. 2014, doi: 10.1109/IEEESTD.2014.6826459.

[35] M. Davari and Y. A.-R.-I. Mohamed, "Robust multi-objective control of VSC-based DC-voltage power port in hybrid AC/DC multi-terminal micro-grids," *IEEE Trans. Smart Grid*, vol. 4, no. 3, pp. 1597–1612, Sep. 2013.

Masoud Davari (Senior Member, IEEE) was born in Isfahan, Iran, in 1985. He received the B.Sc. degree (Hons.) in electrical engineering-power from the Isfahan University of Technology, Isfahan, in 2007, the M.Sc. degree (Hons.) in electrical engineering-power from the Amirkabir University of Technology (Tehran Polytechnic), Tehran, Iran, in 2010, and the Ph.D. degree in electrical engineering-energy systems from the University of Alberta, Edmonton, AB, Canada, in 2016.

He was with the Iran Grid Secure Operation Research Center, Electric Power Research Institute (EPRI), Tehran, from 2010 to 2011. From 2015 to 2017, he was collaborating with Quanta-Technology Company, Markham, ON, Canada, in the field of the dynamic interaction of renewable energy systems with smart grids and control, protection, and automation of microgrids as a Senior Research and Development Specialist and a Senior Consultant. In 2017, he joined the Department of Electrical and Computer Engineering, Allen E. Paulson College of Engineering and Computing, Georgia Southern University, Statesboro, GA, USA, as a tenure-track Assistant Professor. He has developed and implemented several experimental test rigs for both research universities and the industry. He has also authored several IEEE TRANSACTIONS and journals, IET journals, and energies journal. His research interests include the dynamics, controls, and protections of different types of power electronic converters, which are employed in the hybrid ac/dc smart grids, and hardware-in-the-loop (HIL) testing of modernized power systems.

Dr. Davari is an Invited Member of the Golden Key International Honour Society. He has been an active member and a Chapter Lead (for Chapter 3) at the IEEE WG P2004, a newly established IEEE working group on the HIL simulation for the IEEE Standards Association, since 2017. He was an invited reviewer of various IEEE conferences and an invited speaker at different universities and in diverse societies. He served as the Chair of the Literature Review Subgroup of dc@home Standards for the IEEE Standards Association from 2014 to 2015.

Mohammad Pourmahmood Aghababa (Member, IEEE) was born in Tabriz, Iran, in 1983. He received the Ph.D. degree in electrical engineering (major control engineering) from the University of Tabriz, Tabriz, in 2011.

He was a Researcher with the Ecole Centrale de Nantes, Nantes, France. He is currently a Professor with the Urmia University of Technology, Urmia, Iran, and also a Researcher with the University of Windsor, Windsor, ON, Canada. Before joining the University of Windsor, he was a Researcher with the École Centrale de Nantes, Nantes, France. He has authored or coauthored over 90 international ISI-JCR journal articles. He has also authored a book *Advanced Nonlinear Control Systems: Theory, Design and Applications* (in Persian). His current research interests include control theory and application, robotics and mechatronics, machine learning and AI, and fractional-order systems.

Dr. Aghababa has served as a technical committee member for many international conferences. He is an Associate Editor of the *International Journal of Machine Learning and Cybernetics* and the *Journal of Control, Automation and Electrical Systems*. He was recognized as the Youngest Full Professor among all the universities of the Ministry of Science, Research and Technology of Iran in 2018. He has been nominated as one of the best one percent highly cited researchers of the world in the engineering field from 2017 to 2019.

Frede Blaabjerg (Fellow, IEEE) received the Ph.D. degree in electrical engineering from Aalborg University, Aalborg, Denmark, in 1995, and the honoris causa degree from the University Politehnica Timisoara, Timisoara, Romania, in 2017, and the Tallinn University of Technology, Tallinn, Estonia, in 2018.

He was with ABB-Scandia, Randers, Denmark, from 1987 to 1988. He became an Assistant Professor with the Department of Energy Technology, Aalborg University, in 1992, an Associate Professor in 1996, and a Full Professor of power electronics and drives in 1998, where he has been a Villum Investigator since 2017. He has authored or coauthored more than 600 journal articles in the fields of power electronics and its applications, coauthored four monographs, and the edited ten books in power electronics and its applications. His current research interests include power electronics and its applications, such as in wind turbines, photovoltaic systems, reliability, harmonics, and adjustable speed drives.

Dr. Blaabjerg received the 31 IEEE Prize Paper Awards, the IEEE PELS Distinguished Service Award in 2009, the EPE-PEMC Council Award in 2010, the IEEE William E. Newell Power Electronics Award 2014, and the Villum Kann Rasmussen Research Award 2014. He was a recipient of the Global Energy Award for a significant contribution to the development of technologies that provide new opportunities in energy development in 2019. He is the President of the IEEE Power Electronics Society for 2019–2020 and the Vice President of the Danish Academy of Technical Sciences. He was the Editor-in-Chief of the IEEE TRANSACTIONS ON POWER ELECTRONICS from 2006 to 2012. He was a Distinguished Lecturer of the IEEE Power Electronics Society from 2005 to 2007 and the IEEE Industry Applications Society from 2010 to 2011 and 2017 to 2018. He was nominated by Thomson Reuters to be included in the 250 most cited researchers in engineering in the world in 2014–2018.

Mehrdad Saif (Senior Member, IEEE) received the B.S.E.E., M.S.E.E., and D.Eng. degrees from Cleveland State University, Cleveland, OH, USA, in 1982, 1984, and 1987, respectively.

During his graduate studies, he worked on research projects sponsored by the Cleveland Advanced Manufacturing Program, National Aeronautics and Space Administration (NASA) Glenn Research Center, Cleveland, OH, USA. In 1987, he joined as an Assistant Professor with the School of Engineering Science, Simon Fraser University, Burnaby, BC, Canada, where he was the Director of the School of Engineering Science from 2002 to 2011 and led a major expansion of that school during his term. He has been the Dean of the Faculty of Engineering, University of Windsor, Windsor, ON, Canada, since 2011. In this role, he has led significant enrolment growth through strategic enrolment management and the expansion of the Faculty of Engineering programs into areas, such as aerospace engineering, engineering management, B.Eng. technology, mechatronics, and others. He has also overseen significant growth in the number of faculty and research productivity of the Faculty of Engineering. He has been a Consultant to a number of industries and agencies, such as General Motors, Detroit, MI, USA, NASA, Washington, DC, USA, BC Hydro, Vancouver, BC, Canada, Ontario Council of Graduate Studies, Toronto, ON, Canada, and others. His research interests are in systems and control, estimation and observer theory, model-based fault diagnostics, condition monitoring, diagnostics and prognostic, and application of these areas to automotive, power, autonomous systems, and other complex and cyber-physical systems. He has published over 350 refereed journal and conference articles and edited a book in these areas.

Dr. Saif is a fellow of the Canadian Academy of Engineering and the Institution of Engineering and Technology. He is currently a member of the Editorial Board of IEEE ACCESS and the IEEE SYSTEMS JOURNAL. He served as the Chairman of the Vancouver Section of the IEEE Control Systems Society in 1995 and 1997. He is a Registered Professional Engineer in Ontario, Canada.